Final Report

Study of an Objective Performance Measure for Spaceborne Wind Sensors

Maria Belmonte Rivas

Jos de Kloe

Ad Stoffelen

Weather Research

Royal Netherlands Meteorological Institute

De Bilt, November 2009

ESA CONTRACT No. 18041/04/NL/AR

Koninklijk Nederlands
Meteorologisch Instituut
Ministerie van Verkeer en Waterstaat

KNMI

ESA STUDY CONTRACT REPORT

ESA CONTRACT **No. 18041/04/NL/AR**	**SUBJECT** **Study of an Objective Performance Measure for Spaceborne Wind Sensors** **CCN-2: Wind Retrieval Performance Comparison for Post-EPS Scatterometers**		**CONTRACTOR** **Royal Netherlands Meteorological Institute – KNMI (Netherlands)**
ESA CR( )NO	**STAR CODE**	**No. of volumes: 1** **This is Volume No. 1**	**CONTRACTOR'S REFERENCE**

SUMMARY:

The objective of the original study was to develop and consolidate, through simulations and validations using real data, an objective measure of performance for spaceborne wind sensors such as scatterometers and polarimetric radiometers. Three different types of Figure-of-Merit (FoM) have been developed: (1) Wind vector RMS error; (2) Ambiguity susceptibility; (3) Wind biases. Those performance figures were applied to simulate data of the existing QuikScat and ASCAT for validation. Consistent agreement was observed with respect to that of the real data.

CCN-2: The objective of the work extension was to assess the end-to-end wind retrieval performance of the various instrument concepts, which are considered under the industrial Phase 0 studies, using the new FoM, and to allow objective comparison. Two types of scatterometer concepts were considered: an ASCAT-type and RFSCAT-type with varying design parameters. Excellent performance is predicted for both types with the baseline polarisation option of VV. The ASCAT-type concept offers a uniform performance across the swath, while the RFSCAT-type has degraded performance around the nadir and swath edges. The useful swath-width is nevertheless comparable for both concepts.

The work described in this report was done under ESA Contract. Responsibility for the contents resides in the author or organisation that prepared it.

Names of authors: Maria Belmonte Rivas, Jos de Kloe, Ad Stoffelen

NAME OF ESA STUDY MANAGER	**ESA BUDGET HEADING**
Chung-Chi Lin **DIV:** EOP-PI **DIRECTORATE:** Earth Observation	G/1/100.060/600.5100/GE+/RD100/04A21

Abstract - This document defines a set of objective performance metrics (Figures of Merit or FoMs) for the evaluation of various scatterometer configurations in terms of the quality of the retrieved wind estimates. The output wind quality is inferred from the statistical distribution of wind solutions produced by an end-to-end wind retrieval simulator that operates under specified instrumental and geophysical noise conditions.

Table of Contents

0 – Introduction

The aim of the present Post-EPS SCA performance study is the construction of an objective evaluation frame to characterize the wind measurement error incurred by different scatterometer concepts with well-defined beam geometries and radiometric properties. The SCA performance model provides objective support to elaborate on different instrument configuration issues [including fixed or rotating antennas (Fig. 1), number of azimuth views, radiometric performance, single or dual polarization capabilities, and various pulse timing and ground-filter approaches] while monitoring the resulting wind quality.

ASCAT RFSCAT

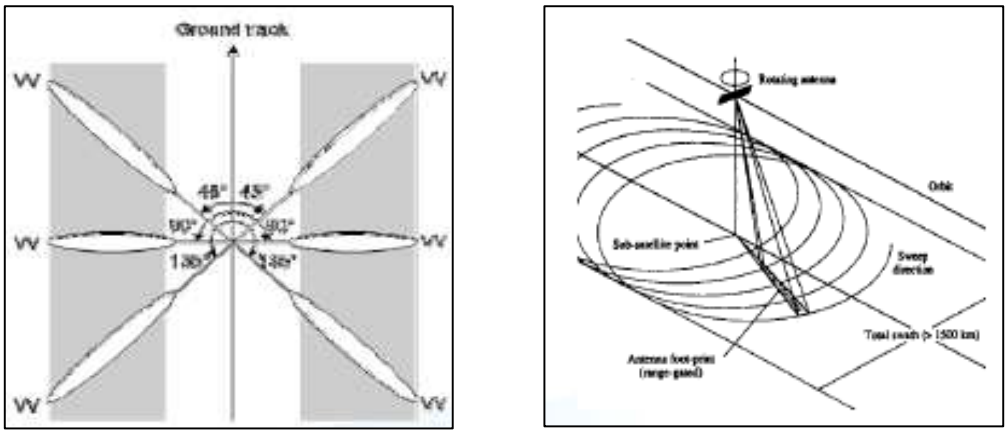

Figure 1 – Post-EPS baseline (fixed beam) and backup (rotating beam) scatterometer concepts

1 – Scatterometer Performance Model

The scatterometer performance model rests on the output wind statistics produced by an end-to-end scatterometer (SCA) wind retrieval simulator, which is programmed in Fortran 90 and schematically shown in Fig. 2 [Lin, 2002]. The SCA wind retrieval simulator converts an input wind vector ($\mathbf{v}_{IN}$) extracted from a world wind climatology into a vector of error/noise-free backscatter coefficient measurements using an empirical Geophysical Model Function (GMF) sampled at observation angles specified by the scatterometer beam geometry. These backscatter

components are corrupted by as much noise as specified by the system (instrumental + geophysical) noise levels, and injected to the wind retrieval core of the simulator to generate an output wind vector ($\mathbf{v}_{OUT}$). After a large number of wind inversions (or MonteCarlo runs), the output wind solutions are collected and binned into output wind distribution functions $P_{obs}(\mathbf{v}_{OUT}|\mathbf{v}_{IN})$, which describe the statistical distribution of wind outputs for a particular wind input and allow the characterization of the retrieval error incurred by a particular scatterometer concept via mean statistics such as the wind vector root-mean-square error, the wind vector bias or the presence of multiple ambiguous solutions. The following sections describe in detail how these processes are implemented.

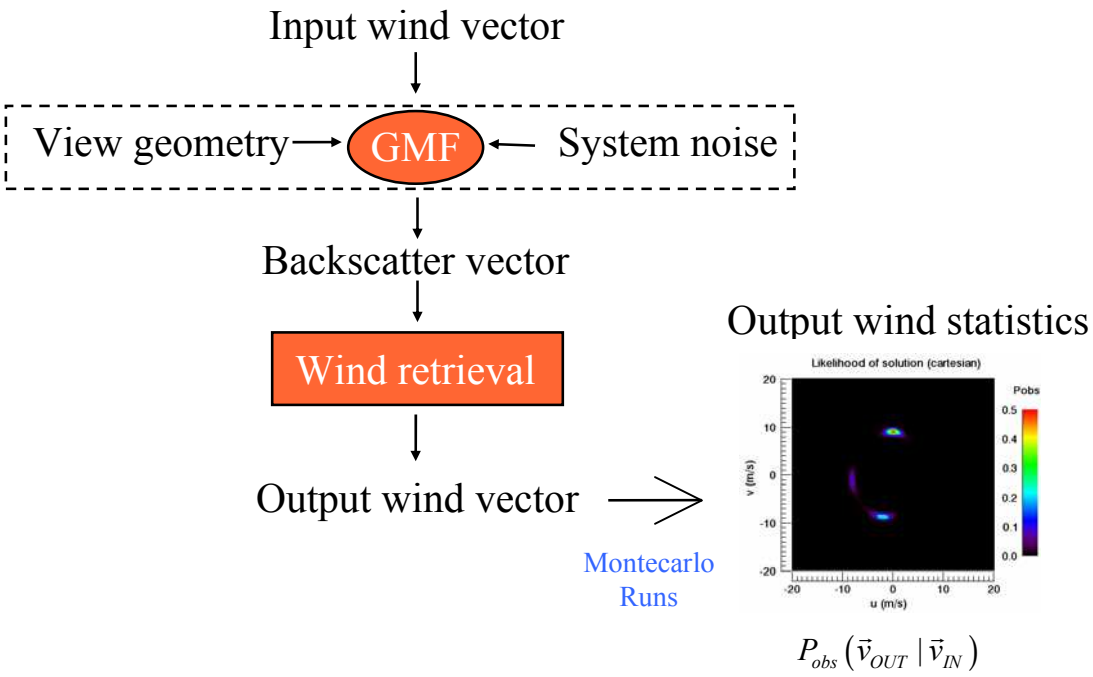

Figure 2 – End-to-end scatterometer performance model

1.1 Input wind

The retrieval of ocean wind vectors in scatterometry is a non-linear problem and the error characteristics of the wind output depend on the wind input state. To eliminate this undesirable dependence on initial conditions, the scatterometer error characteristics are to be averaged over a world climatology of wind inputs characterized by a Weibull distribution in wind speeds [Liu, 2008] with a maximum around 8 m/s (see Fig. 3) and a uniform distribution in wind direction. The input wind speeds are discretized from 3 to 16 m/s using steps of 1 m/s, covering about 90 %

of ocean wind states. The input wind directions are discretized from 0 to 360 degrees using steps of 10 degrees.

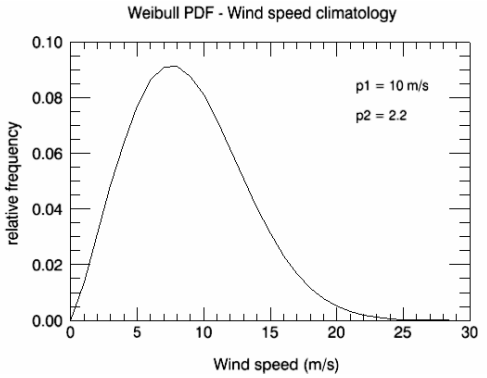

$$f(v) = \frac{p2}{p1}\left(\frac{v}{p1}\right)^{p2-1} e^{-\left(\frac{v}{p1}\right)^{p2}}$$

Figure 3 –Wind speed climatology (Weibull PDF, p1=10 & p2=2.2 [Liu, 2008])

1.2 Geophysical model function

The geophysical model function (GMF) is an empirically derived function that relates backscatter measurements to surface wind vectors and viewing geometries in the form of σ^0 = GMF (incidence angle, azimuth angle, wind vector). For C-band VV simulations, we use the CMOD5 model for ocean backscatter [Hersbach, 2007], which is valid for incidence angles ranging from 18 to 58 degrees. For Ku-band VV and HH simulations, we use the NSCAT backscatter numerical tables [Wentz, 1999].

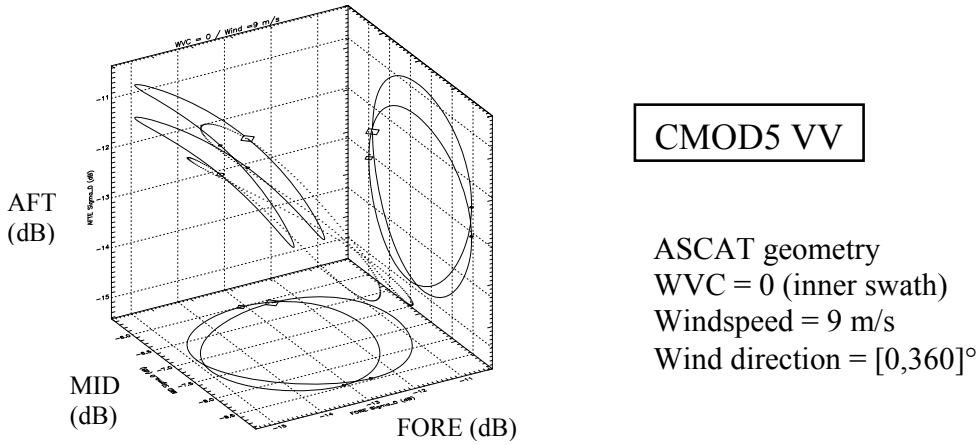

Figure 4A – CMOD5: C-band GMF in ASCAT measurement space (3 views)

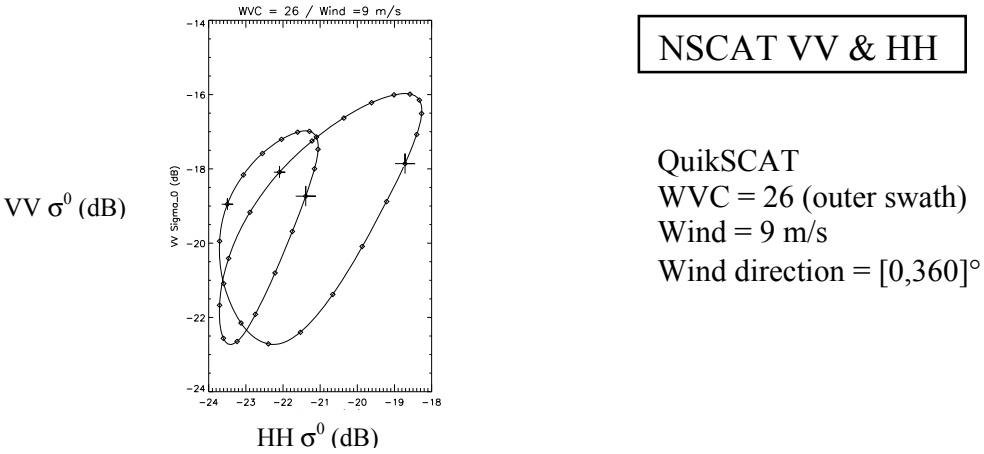

Figure 4B – NSCAT: Ku-band GMF in QuikSCAT measurement space (4 views)

1.3 Observation geometry

The correct determination of the ocean wind vector signature requires that every resolution cell (WVC node) on the surface be visited by a number of views from a diversity of observation angles. The observation geometry refers to the sequence of view (incidence and azimuth) angles at which the scatterometer beams intersect the surface, which is in general a function of the across-track distance of the WVC node, and of the beam rotation speed and timing for a rotating system. The observation geometry is calculated for every node on the swath using a simplified orbital model together with specific scatterometer instrument model parameters, and written to "Pseudo-Level 1b" files (see Fig. 5a).

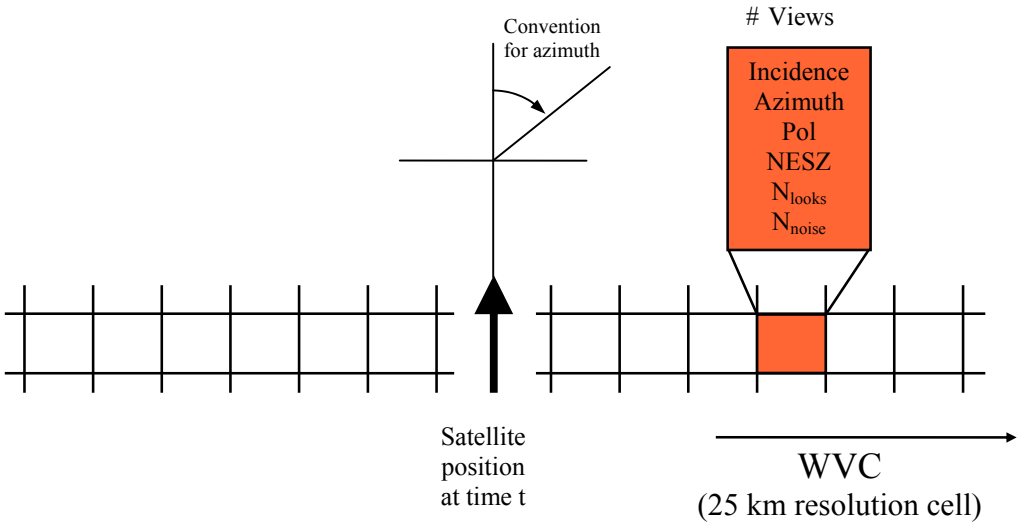

Figure 5a – Pseudo Level 1b file information

The Pseudo-Level 1b file is generated by simulators developed by the phase 0 industrial study teams, who are designing the scatterometer system. Other relevant information stored in Pseudo-Level 1b files are the transmitted polarization, the single look Noise-Equivalent-Sigma-Zero (NESZ = σ^0/SNR, also known as sensitivity), and the number of independent signal and noise looks (N_{looks}, N_{noise}) averaged per view (see Fig. 5b). The NESZ or sensitivity describes how the transmit power is distributed over the scatterometer swath as a function of total transmit power, TX/RX antenna pattern, slant range and system bandwidth. A description of the scatterometer observation geometries used in this study (QuikSCAT, ASCAT and RFSCAT) can be found in Appendix A.

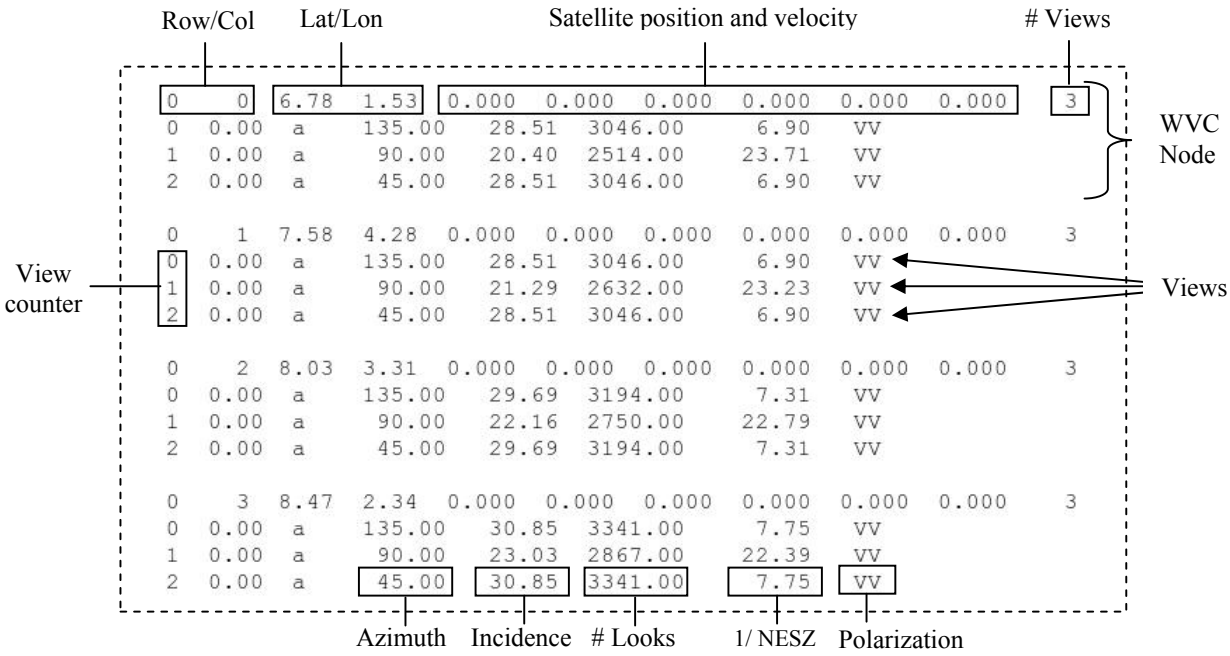

Figure 5b – Pseudo Level 1b file structure

1.4 System noise

The system noise comprises both instrumental and geophysical components. The instrumental noise sets the system radiometric resolution and it is modeled following [Fischer, 1972] as

$$k_p^2 = \frac{\mathrm{var}\{\sigma^0\}}{\left(\sigma^0\right)^2} = \frac{1}{N_{looks}}\left(1+\frac{1}{SNR}\right)^2 + \frac{1}{N_{noise}SNR^2} \qquad [1]$$

where N_{looks} and N_{noise} refer to the number of independent signal and noise looks averaged per view, and SNR refers to the average Signal to Noise Ratio for a single look (= σ^0/NESZ). The geophysical noise model is empirically adjusted to observed ASCAT and QuikSCAT <MLE> tables at 50 km resolution (see Appendix B) and modeled as a function of wind speed as:

$$\textit{C-band} \qquad k_{geo}(v) = 0.12\exp(-v/12)$$

$$\textit{Ku-band} \qquad k_{geo}(v) = 0.05 + 2.2 \cdot e^{-v/2} \qquad [2]$$

The instrumental and geophysical noise contributions are assumed Gaussian and uncorrelated. For simulated observations, the total backscatter noise is modeled as

$$\sigma^0 = \sigma^0_{GMF}\left(1 + \sqrt{k_p^2 + k_g^2} \cdot N[0;1]\right) \qquad [3]$$

where N[0,1] is a Gaussian PDF with zero mean and unit standard deviation.

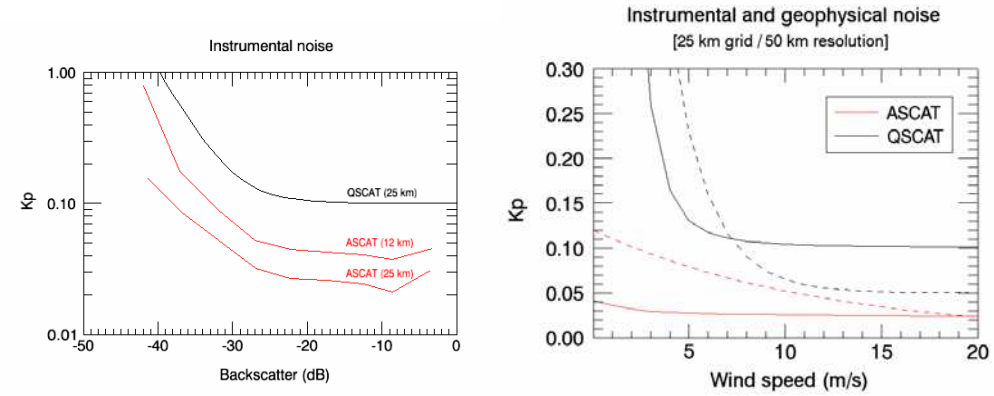

Figure 6 – Representative instrumental (continuous) and geophysical (dashed) noise levels at C and Ku-band (instrumental noise as reported in KNMI/NOAA BUFR products)

Figure 6 displays typical levels of instrumental and geophysical noise observed by the QuikSCAT and ASCAT scatterometers. ASCAT backscatter noise levels are consistent with the current 3-to-10 % Kp requirement for the nominal mode (50 km resolution or 25 km gridding) at min/max backscatter conditions (i.e. low cross-wind in outer swath and high up-wind in inner swath).

1.5 Wind retrieval

The retrieval of ocean winds from scatterometer data relies on the use of empirically derived Geophysical Model Functions (GMFs), which relate the state variables wind speed and wind direction to backscatter measurements. The wind inversion is based on a search for minimum distances between backscatter measurements and backscatter model solutions lying on the

empirical GMF surface. We define the normalized square distance MLE($\mathbf{v}|\sigma^0$) from backscatter observations σ^0 to backscatter wind solutions $\sigma^0_{GMF}(\mathbf{v})$ on the GMF surface as:

$$MLE(\vec{v} \mid \sigma^0) = \frac{1}{\langle MLE \rangle} \sum_{i=1\ldots N} \frac{\left|\sigma_i^0 - \sigma^0_{GMF,i}(\vec{v})\right|^2}{\mathrm{var}\{\sigma_i^0\}} \qquad [4]$$

where N is the dimension of the backscatter vector (i.e. the number of views per WVC node), var$\{\sigma^0\}$ is the instrumental noise variance and <MLE> is an empirical normalization factor that accounts for deviations from the ocean wind GMF due to geophysical noise, namely sub-cell wind variability and/or rain contamination. The normalized square distance MLE is but a sum of weighted square residuals between model and observed backscatter vectors, and the wind inversion consists of a search for minimum MLE across the space of solutions. The backscatter point on the GMF surface that lies the closest to observations yields the wind output, also known as the *first rank wind solution*.

Assuming Gaussian noise in the backscatter components, the minimum normalized square distance MLE_{min} in Eq. [4] becomes the sum of the squares of N standard normal *but not all independent* variables (see Appendix C). A correlation among the sum components is introduced by projection constraints, meaning that noise excursions along the GMF model do not contribute to MLE. If wind retrieval were a linear problem, the probability that a backscatter vector lay at a normalized square distance MLE away from the two-dimensional GMF plane would thus follow a chi-square distribution with N-2 *independent* degrees of freedom, where the remaining two degrees of freedom push the first rank wind solution around the true wind on the GMF plane without MLE penalization (see Figure 7).

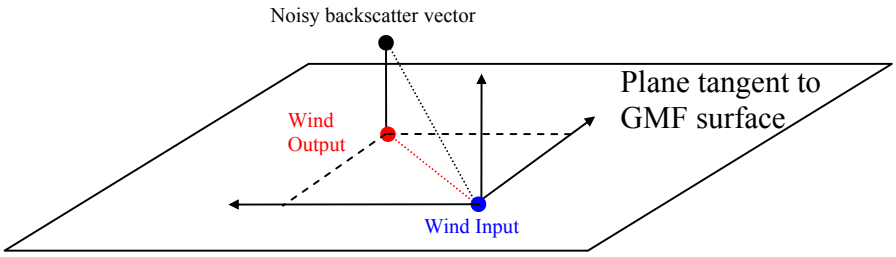

Figure 7 – Radiometric noise projections across and along the plane tangent to the GMF surface.

Thus for a linear inversion problem, the distribution of minimum MLE residuals across the GMF for first rank wind solutions could be modeled as

$$P(MLE_{\min}) = \chi^2_{N-2}[MLE_{\min}] \qquad [5]$$

while the distribution of first rank wind solutions about the true wind could be modeled as

$$P_{obs}(\vec{v} \mid \vec{v}_0) = \chi^2_2\left[MLE(\vec{v} \mid \vec{v}_0)\right] \qquad [6]$$

where MLE($\mathbf{v}|\mathbf{v}_0$) refers to *special* noise excursions along the two-dimensional GMF surface:

$$MLE(\vec{v} \mid \vec{v}_0) = \sum_{i=1\ldots N} \frac{\left|\sigma^0_{GMF,i}(\vec{v}_0) - \sigma^0_{GMF,i}(\vec{v})\right|^2}{\mathrm{var}\{\sigma^0_{GMF,i}(\vec{v}_0)\}} \qquad [7]$$

Thus at least in theory, Eq. [5] characterizes the spread of observations across the GMF surface in the space of measurements while Eq. [6] characterizes the spread of outputs about the true input in the space of solutions. In reality, the GMF surface bends and folds non-linearly in the space of measurements (see Fig.4), whereby large noise excursions may cause first rank solutions to land on nearby GMF branches or protuberances, resulting in multiple ambiguous and/or biased wind retrievals. For large noise excursions (or highly non-linear cases) the analytical chi-square approximations just described loose their validity and a numerical Monte Carlo approach is prescribed to simulate more realistic output wind statistics. At lower noise levels, the analytical chi-square approximations serve as stringent end-to-end simulator verification tools (Section 3).

These concepts are illustrated in Fig. 7 and Fig. 8 for QuikSCAT and ASCAT instrument types, respectively. The left panels display the *special* normalized square distances MLE($\mathbf{v}|\mathbf{v}_0$) to a perfect measurement $\sigma^0_{GMF}(\mathbf{v}_0)$ on the GMF surface. The right panels display the corresponding output wind statistics $P_{obs}(\mathbf{v}|\mathbf{v}_0)$ calculated from Eq. [6]. The only probable wind solutions are those whose backscatter distances to the true wind are commensurate with the system noise levels.

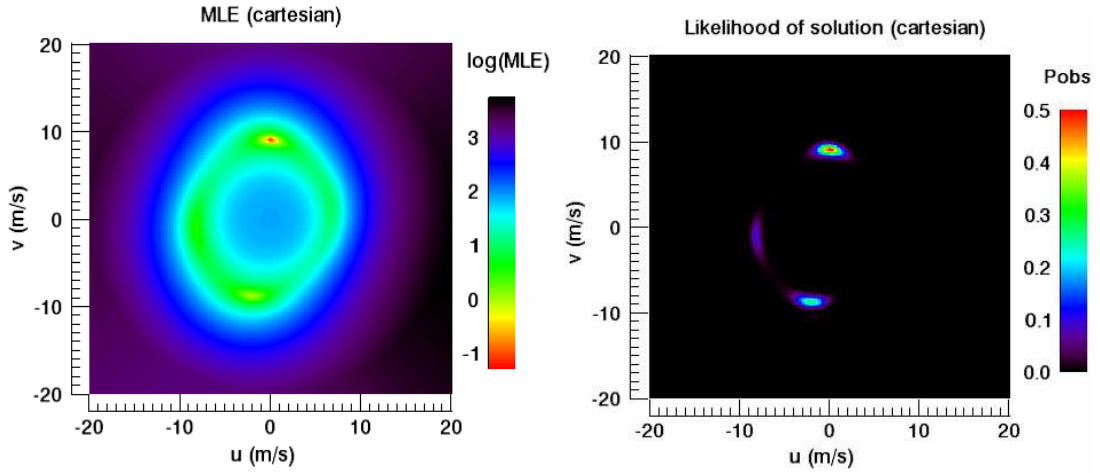

Figure 7 – Chi-square MLEs (left, from Eq. [4]) and output wind statistics (right, from Eq. [5]) for QuikSCAT outer swath (WVC 26) with input wind 9 m/s @ 90° , k_p = 10 % and <MLE>=5

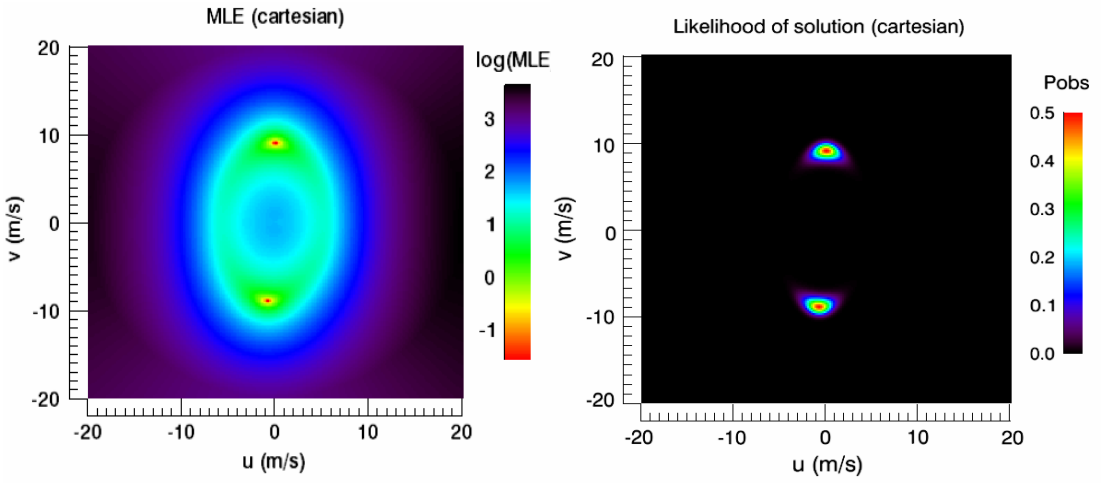

Figure 8 – Chi-square MLEs (left, from Eq. [4]) and output wind statistics (right, from Eq. [5]) for ASCAT outer swath (WVC 20) with input wind 9 m/s @ 90° and k_p = 10 % with <MLE>=5

Note that the scatterometer wind retrieval performance is affected by the presence of multiple ambiguous solutions, which arise from a combination of instrumental noise, some non-ideal observation geometries and proximity between the GMF up- and downwind branches. The process of selecting a wind solution among a set of likely candidates is called ambiguity removal, and the method used at KNMI (see e.g. 2DVAR [Vogelzang, 2009]) draws from Numerical Weather Prediction (NWP) model information for this purpose. The problem is solved by minimizing a total cost function that combines both observational and NWP background contributions as:

$$J = -2\ln(probability) = J_{obs} + J_{NWP} = -2\ln\left(P_{obs}(\vec{v} \mid \vec{v}_0) \cdot P_{NWP}(\vec{v} - \vec{v}_{NWP})\right) \quad [8]$$

Which in terms of probabilities is equivalent to the product of the simulator output wind statistics $P_{obs}(\mathbf{v}|\mathbf{v}_0)$ times a Gaussian probability distribution $P_{NWP}(\mathbf{v}\text{-}\mathbf{v}_{NWP})$ centered about a NWP "true" wind forecast with a variance $\sigma_{NWP}^2 \sim 5$ m^2/s^2 in the wind components, resulting in an ambiguity-free output wind distribution function $P_{obs}(\mathbf{v}|\mathbf{v}_0)P_{NWP}(\mathbf{v}\text{-}\mathbf{v}_{NWP})$ (see Fig. 9). The NWP forecast variance σ_{NWP} has been chosen to be commensurate with the sum of the NWP model analysis and representativeness errors. Also, note that in operational practice, the observational contribution to the ambiguity removal procedure in Eq. [8] is drawn from $P_{obs}(\text{MLE}(\mathbf{v}))$ defined in Eq. [5] instead of $P_{obs}(\mathbf{v}|\mathbf{v}_0)$ due to poor knowledge of the true wind.

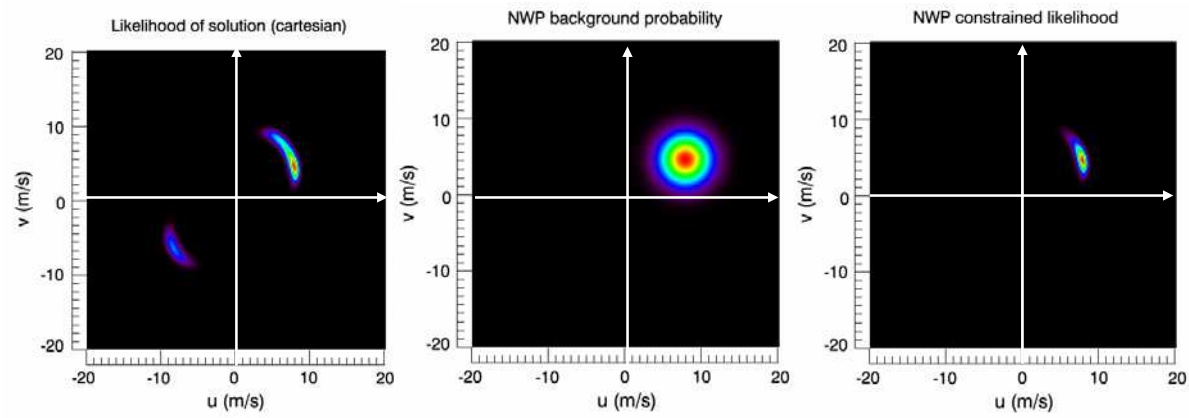

Figure 9a – Ambiguity removal in the end-to-end scatterometer performance model: Output wind statistics (left); NWP probability (center); ambiguity-free output wind statistics (right) for QuikSCAT outer swath (WVC 26) with input wind 9 m/s @ 30° and k_p = 10 % with <MLE>=5

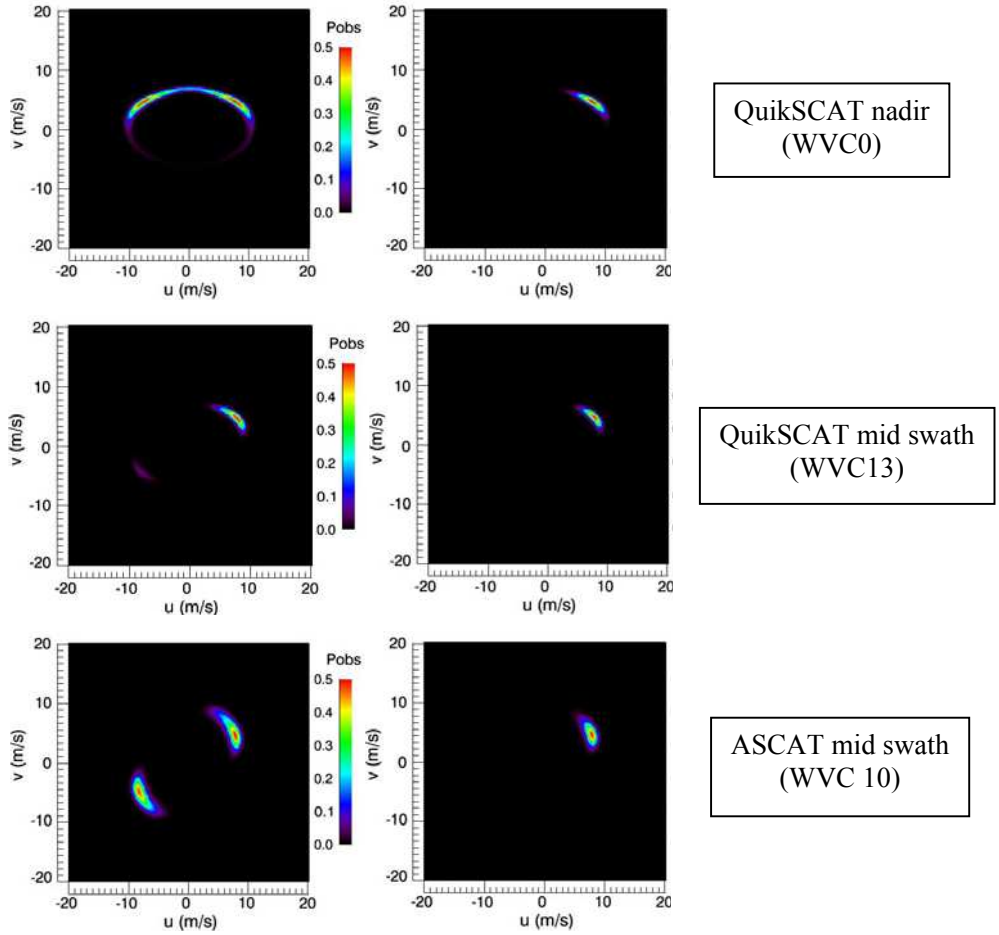

Figure 9b – Simulator output wind statistics before (left) and after ambiguity removal (right), for input wind 9 m/s @ 30° and k_p = 10 % with <MLE>=5

2 – Figures of Merit

The objective of the Figures of Merit (FoMs) is to allow the comparison of different SCA concepts and configurations on grounds of wind retrieval quality, in a way such that imprecise, ambiguous and biased wind solutions are penalized. Three separate performance metrics are introduced.

2.1 Wind Vector RMS error

At NWP centers, the quality of a wind measurement is usually referred to a vector RMS error. Along this line, our first FoM is defined as the wind vector RMS error calculated from the ambiguity-free output wind distribution and normalized by the NWP background uncertainty as:

$$FoM_{VRMS} = \frac{RMS_{obs}}{RMS_{NWP}} \subset [0,1] \qquad [9]$$

where

$$RMS_{obs} = \left(\int \left| \vec{v} - \vec{v}_{true} \right|^2 P_{obs}(\vec{v} \mid \vec{v}_{true}) P_{NWP}(\vec{v} - \vec{v}_{true}) d^2 v \right)^{1/2}$$
$$RMS_{NWP} = \left(\int \left| \vec{v} - \vec{v}_{true} \right|^2 P_{NWP}(\vec{v} - \vec{v}_{true}) d^2 v \right)^{1/2} = \sqrt{2}\sigma_{NWP} \qquad [10]$$

and

$$P_{obs}(\vec{v} \mid \vec{v}_{true}) = C\chi_2^2[MLE(\vec{v} \mid \vec{v}_{true})] \qquad [11]$$

$$P_{NWP}(\vec{v} - \vec{v}_{true}) = \frac{1}{2\pi\sigma_{NWP}^2} \exp\left(\left| \vec{v} - \vec{v}_{true} \right|^2 / (2\sigma_{NWP}^2) \right) \qquad [12]$$

The constant C in Eq. [11] guarantees that the integral area under P_{obs}*P_{NWP} is unity. This FoM quantifies the standard deviation of output wind solutions about the true wind after NWP-based ambiguity removal and it should be as low as possible.

2.2 Ambiguity susceptibility

Another performance figure should quantify the ability of a scatterometer to handle ambiguous solutions or function without a priori NWP model information. Our next FoM is defined as the fraction of solutions that fall outside the NWP background constraint (a Gaussian distribution with a variance of 5 m^2/s^2 about the true wind) relative to the number of solutions that fall within it (see Fig. 10), expressed as:

$$FoM_{AMBI} = P_{NWP,\max} \int P_{obs}(\vec{v} \mid \vec{v}_{true}) d^2 v - 1 \subset [0, \infty] \qquad [13]$$

This figure somehow quantifies the importance of NWP model information for scatterometer wind retrieval (i.e. ambiguity removal) and it should be as low as possible.

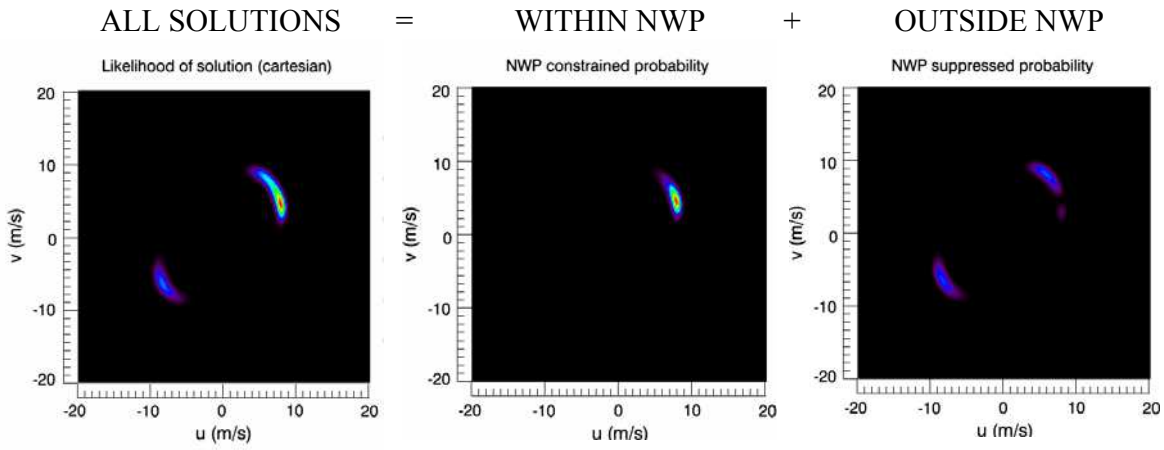

Figure 10a – Output wind statistics $P_{obs}(\mathbf{v}|\mathbf{v}_0)$ (left); ambiguity-free solutions $P_{obs}(\mathbf{v}|\mathbf{v}_0)P_{NWP}(\mathbf{v}-\mathbf{v}_{NWP})$ (center); NWP suppressed solutions $P_{obs}(\mathbf{v}|\mathbf{v}_0)(P_{NWP,max} - P_{NWP}(\mathbf{v}-\mathbf{v}_{NWP})$ (right), for QuikSCAT outer swath (WVC 26) with input wind 9 m/s @ 30° and k_p = 10 % with <MLE>=5

2.3 Wind biases

Systematic errors (biases) arise from degrees of asymmetry (or skewness) in the output wind statistics functions, which cause the mean of the distribution (or average location of the output wind solution) to be shifted from the distribution mode (or location of the true wind, see Figure 11). Systematic wind biases can be calculated along the wind radial and azimuth directions as:

$$bias_{spd} = v_{true} - \int v \cdot P_{obs}(\vec{v} \mid \vec{v}_{true}) P_{NWP}(\vec{v} - \vec{v}_{true})\Big|_{\phi=\phi_{true}} dv$$

$$bias_{dir} = \phi_{true} - \int \phi \cdot P_{obs}(\vec{v} \mid \vec{v}_{true}) P_{NWP}(\vec{v} - \vec{v}_{true})\Big|_{|v|=|v_{true}|} d\phi \qquad [14]$$

Because systematic errors along the wind radial direction (output windspeed biases) are small in general, we will not consider them further in this report. However, the presence of systematic

errors along the wind azimuth direction (output wind direction biases) produces artificial directional preferences that may corrupt the observed wind climatologies (see, e.g. QuikSCAT case in Section 4.1).

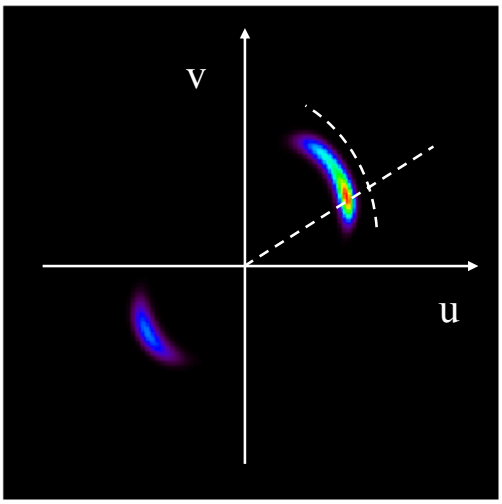

Figure 11 – Skewed output wind statistics give way to systematic biases in wind speed and most notably, in wind direction. In this example, the true wind lies at 9 m/s @ 30 degrees but the wind outputs seem drawn to a 45 degrees solution (QuikSCAT, WVC = 26)

3 – Performance Model Validation

Our scatterometer performance evaluation is based on the Figures of Merit defined above, which are directly calculated from the SCA simulator output wind statistics. We begin by verifying the wind retrieval properties of the SCA end-to-end simulator, namely the distribution of output wind solutions across and along the GMF against the expected approximate chi-square model expressions Eq. [5] and Eq. [6] in Section 1.5. The SCA end-to-end simulator settings are specified in Table 1 below. The simulator inputs include the scatterometer beam geometry, the beam radiometric resolution and the true wind speed. Inversion outputs include the first rank wind solution and its normalized square distance MLE. The wind retrieval scenarios simulated in this section correspond to the QuikSCAT and ASCAT scatterometer concepts with 50 km resolution and representative system (instrumental and geophysical) noise levels as specified in Section 1.4.

Table 1 – SCA end-to-end simulator settings

ITEM	Value	Comments
Pseudo L1B file	ASCAT/QuikSCAT/RFSCAT	Variable Kp
Wind source	constant u,v	World climatology
# simulations	1000 per WVC node	Monte Carlo runs
WVC resolution	50	Affects geophysical noise
Geophysical noise	ON	OFF for MLE statistics
<MLE> normalization	No	
# output solutions	1	First rank solution
Output file name	Reflects input settings	

3.1 MLE statistics

Figure 12 shows the distribution of normalized square distances (MLE) of first rank wind solutions retrieved by the SCA simulator against the analytical chi-square model of Eq. [5]. The agreement between the simulated and analytical MLE distributions is excellent at low noise levels (i.e. Kp ~ 5 %), degrading only slightly as noise levels increase due to the breakdown of the GMF tangent plane approximation. The SCA simulator works as expected as far as MLE statistics are concerned.

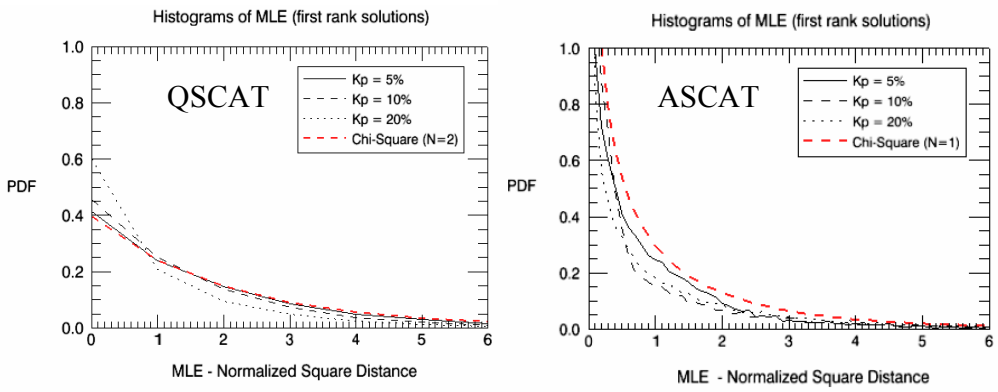

Figure 12 - MLE statistics from the SCA wind retrieval simulator against the expected chi-square distribution with two (QuikSCAT, left) and one (ASCAT, right) degrees of freedom

3.2 Output wind statistics

The retrieved output wind statistics depend on the scatterometer concept, the system noise, the input wind vector and the across-track location of the resolution cell (WVC number). Figures 13 and 14 show chi-square model (left column) versus SCA simulator output wind statistics (right column) for a fixed input wind vector (9 m/s at 45 degrees) at different locations across the QuikSCAT and ASCAT swaths, respectively.

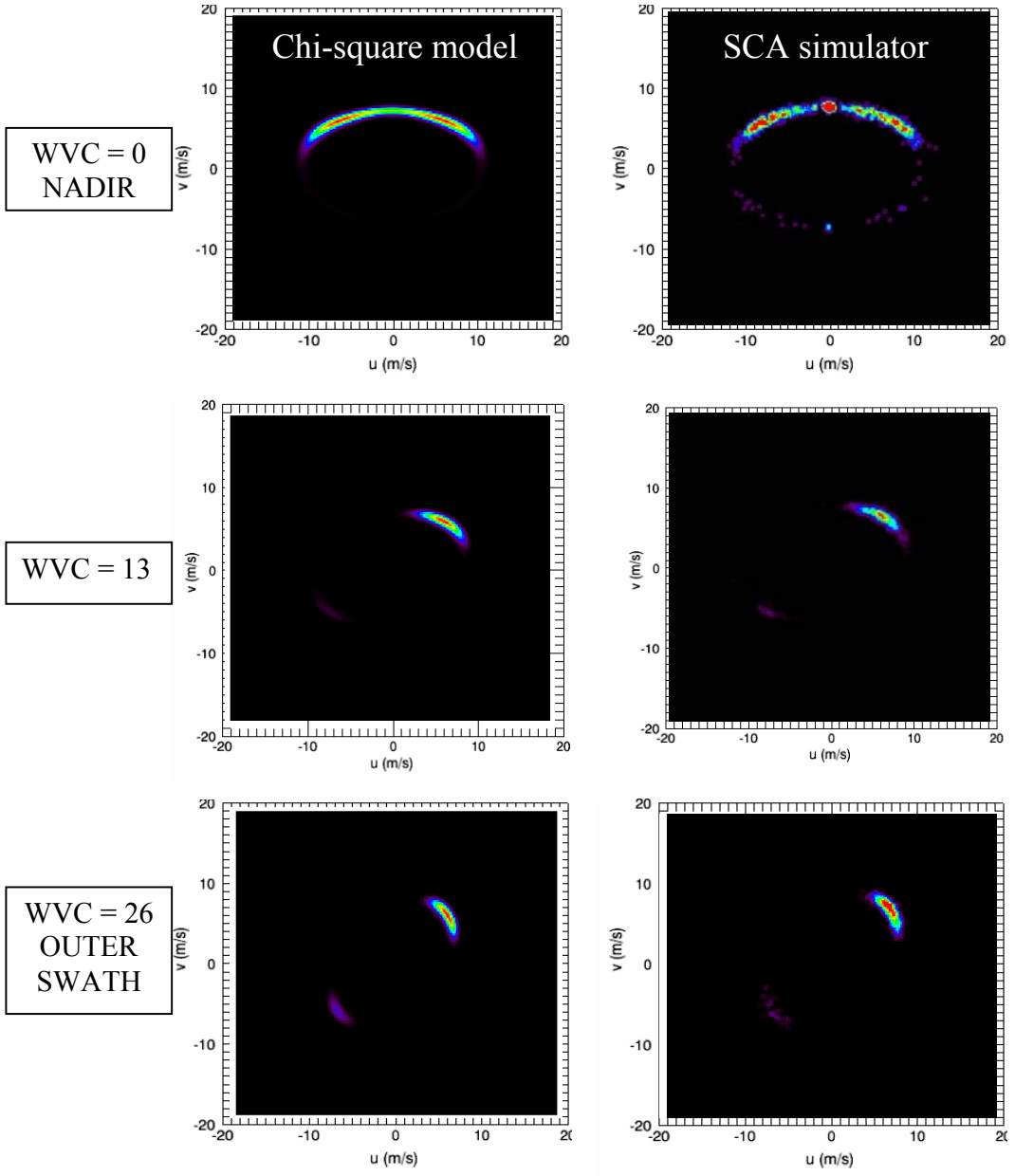

Figure 13 – QSCAT output wind statistics: Chi-square model with two degrees of freedom (left column) against SCA simulator (right column) - input wind is 9 m/s@45 deg with Kp = 22 %

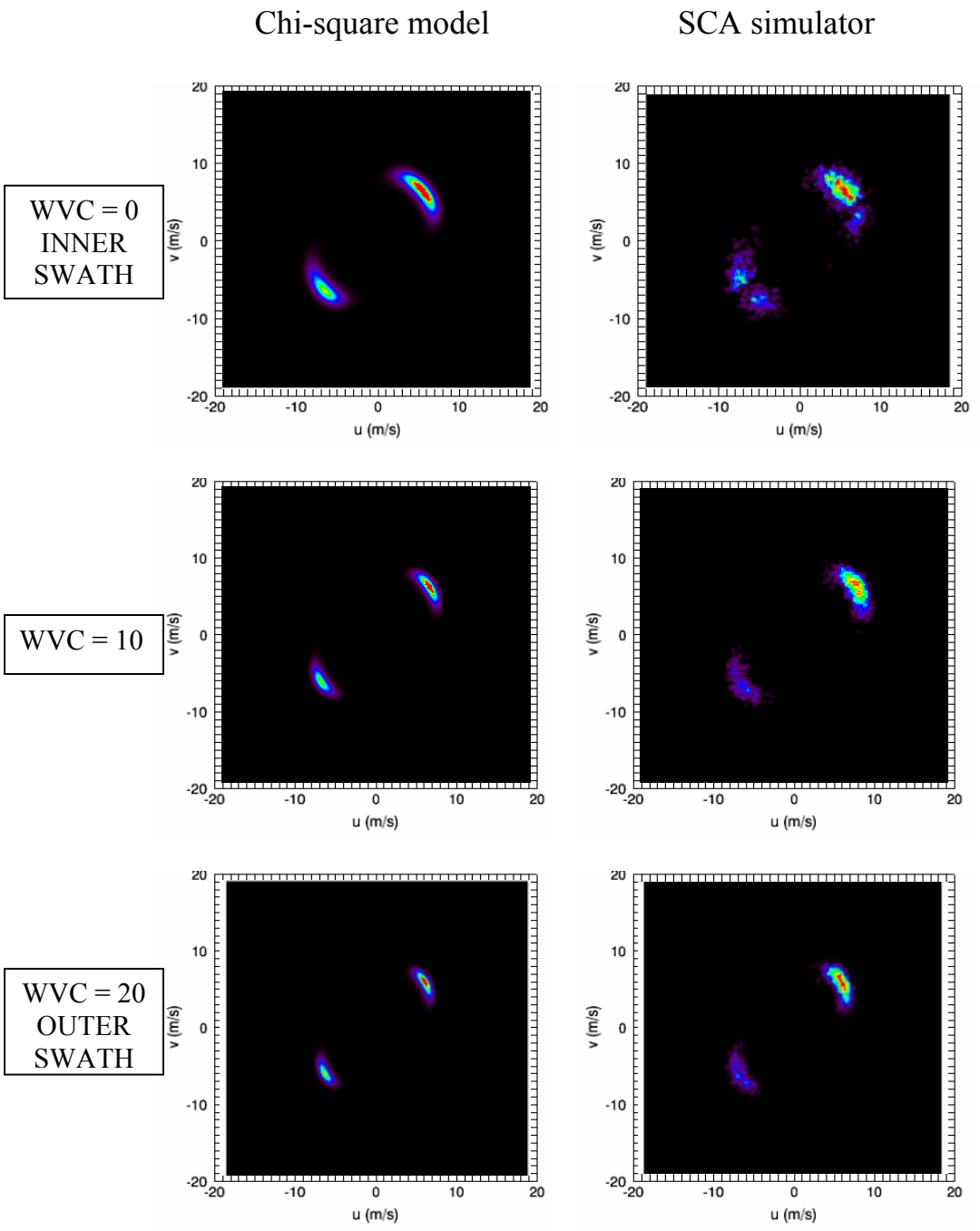

Figure 14 – ASCAT output wind statistics: Chi-square model with two degrees of freedom (left column) against SCA simulator (right column) - input wind is 9 m/s@45 deg with Kp = 22 %

The agreement between the simulated and analytical output wind distributions is excellent at low noise levels (not shown). At larger noise levels (i.e. Kp ~ 20 %), non-linear estimation effects appear as attractor/repulsor solutions that linear chi-square models are not able to reproduce (e.g. see attractor at 90 degrees for QuikSCAT nadir WVC locations in Fig. 13 and repulsor at 30 degrees for ASCAT inner swath cells in Fig. 14). The SCA simulator works realistically as far as the output wind statistics and concomitant retrieval non-linearities are concerned.

3.3 Figures of merit

The statistical distribution of scatterometer wind outputs in the space of solutions determines the output wind vector RMS error, its retrieval ambiguity and the directional bias as defined in Section 2. The non-linear nature of the wind estimation process is reflected in performance metrics that depend on input wind. Figures 15 to 18 show how the scatterometer performance metrics depend on the input wind vector and across-track location of the WVC node respectively for QuikSCAT and ASCAT scatterometer concepts. The performance metrics (labeled VRMS, AMBI and BIAS) are calculated from output wind statistics derived from the chi-square models and actual SCA simulator outputs for comparison.

One can observe that the agreement between the performance metrics derived from the chi-square model and the actual SCA simulator is very good with regard to wind vector RMS error (VRMS). However, discrepancies appear concerning ambiguities and directional biases (AMBI and BIAS), which seem to be mainly driven by GMF non-linearities. The utilization of a statistical Monte Carlo approach using the end-to-end SCA simulator, which we now consider validated, is therefore necessary to fully account for non-linear effects in wind estimation using scatterometers.

A few comments on QuikSCAT and ASCAT performance dependence on wind direction should be made. First, note that the QuikSCAT VRMS figures are worst at nadir cells, particularly for winds blowing along the satellite track (i.e. along the beams). This problem is caused by an observation degeneracy that cannot resolve across-track wind components, leading to solutions that are symmetric with respect to the beam axes. Also, note the presence of strong biases associated with attractor solutions along this axis of symmetry, namely at 90 and 270 degrees. In contrast to QuikSCAT, ASCAT performance is rather uniform in terms of wind direction, with worst performance figures for winds along the ±45 degree diagonals (i.e. along the for/aft beams).

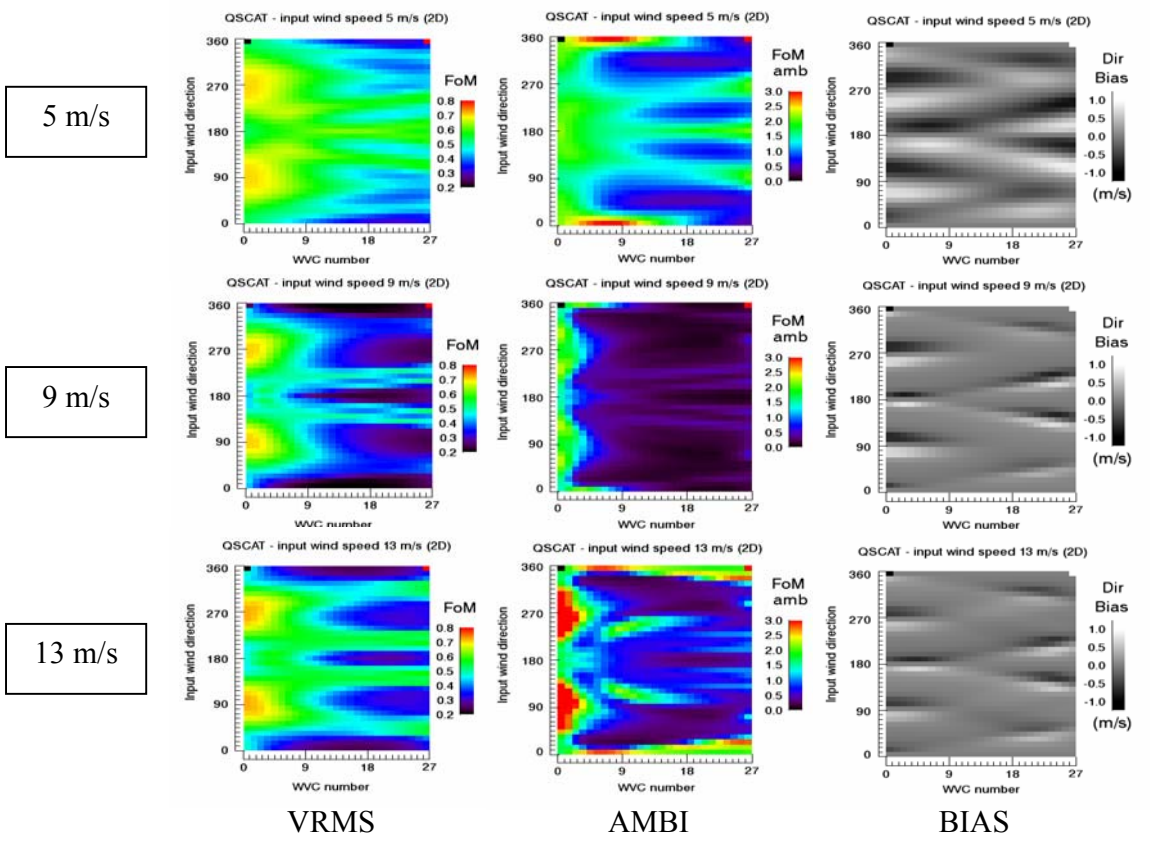

Figure 15 – QSCAT Chi-Square FoMs as a function of wind speed (5, 9, 13 m/s) and direction

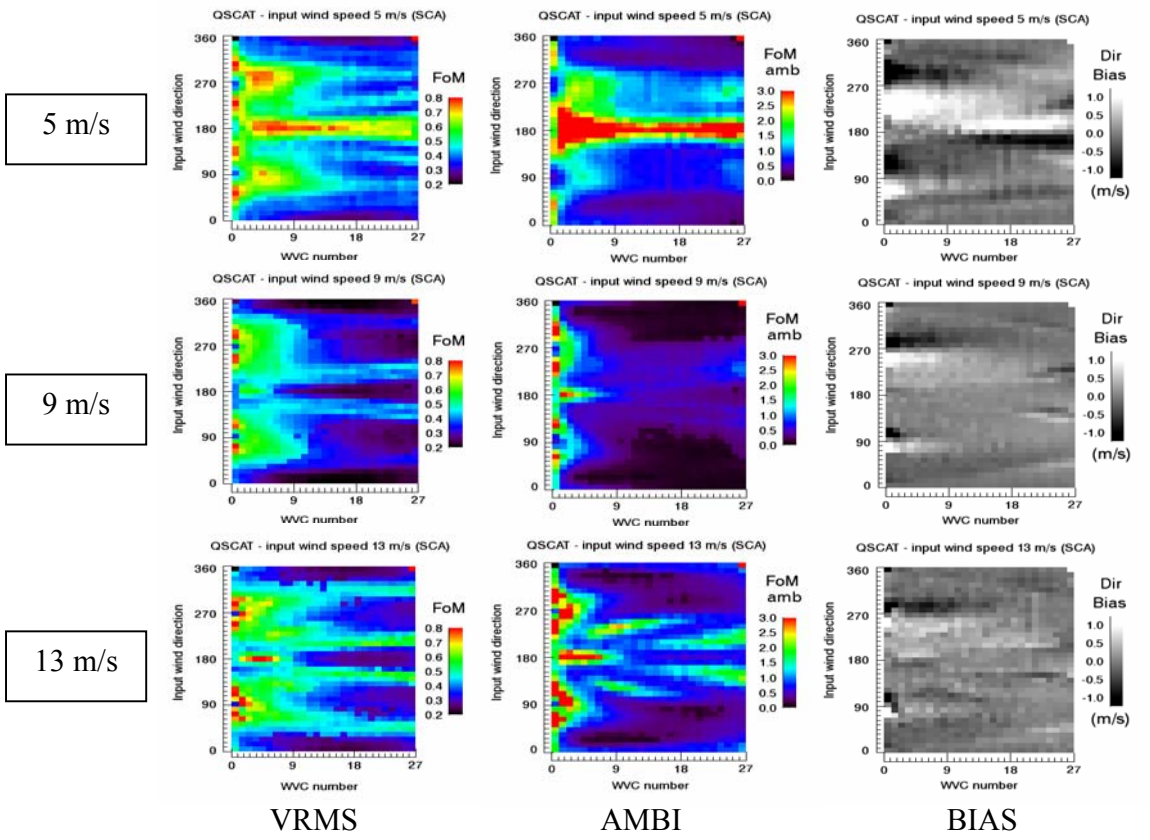

Figure 16 – QSCAT SCA simulator FoMs as a function of wind speed (5, 9, 13 m/s) and direction

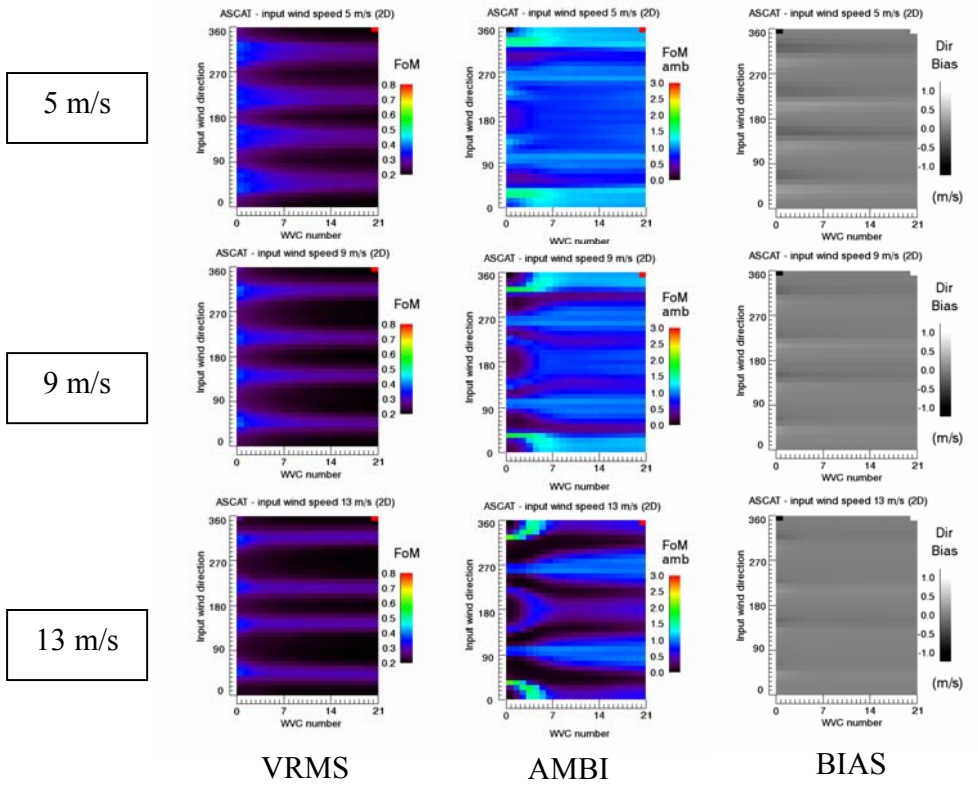

Figure 17 – ASCAT Chi-Square FoMs as a function of wind speed (5, 9, 13 m/s) and direction

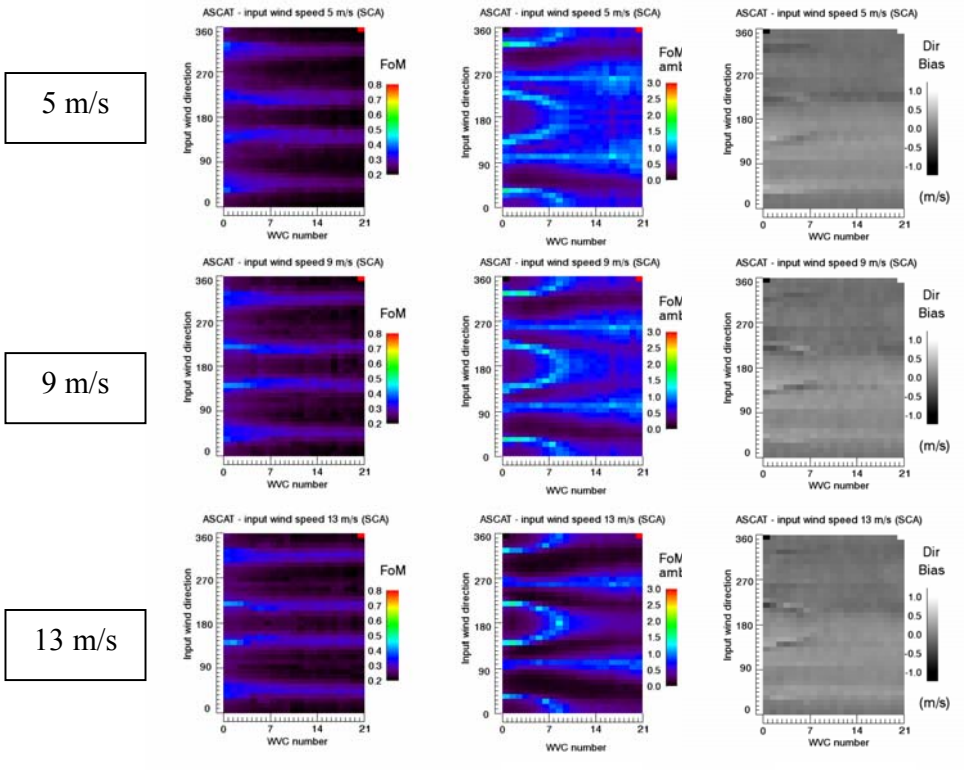

Figure 18 –ASCAT SCA simulator FoMs as a function of wind speed (5, 9, 13 m/s) and direction

4 – Scatterometer Concept Evaluation

To facilitate a straightforward comparison between scatterometer concepts, figures of merit are calculated and then averaged over a climatology of wind inputs as described in Section 1.1. This section describes the resulting climatology performance curves as a function of across-track location, initially for two known instruments (SeaWinds on QuikSCAT and ASCAT on *MetOp*) and finally for the baseline and backup Post-EPS scatterometer concepts (ASCAT-type and RFSCAT-type).

4.1 QuikSCAT vs. ASCAT (50 km)

Figures 19 and 20 summarize the resulting performance figures for SeaWinds on QuikSCAT and ASCAT on *MetOp* using representative instrumental and geophysical noise levels and a spatial resolution of 50 km (i.e. high wind Kp of 10 % for QuikSCAT versus Kp of 3 % for ASCAT on *MetOp*).

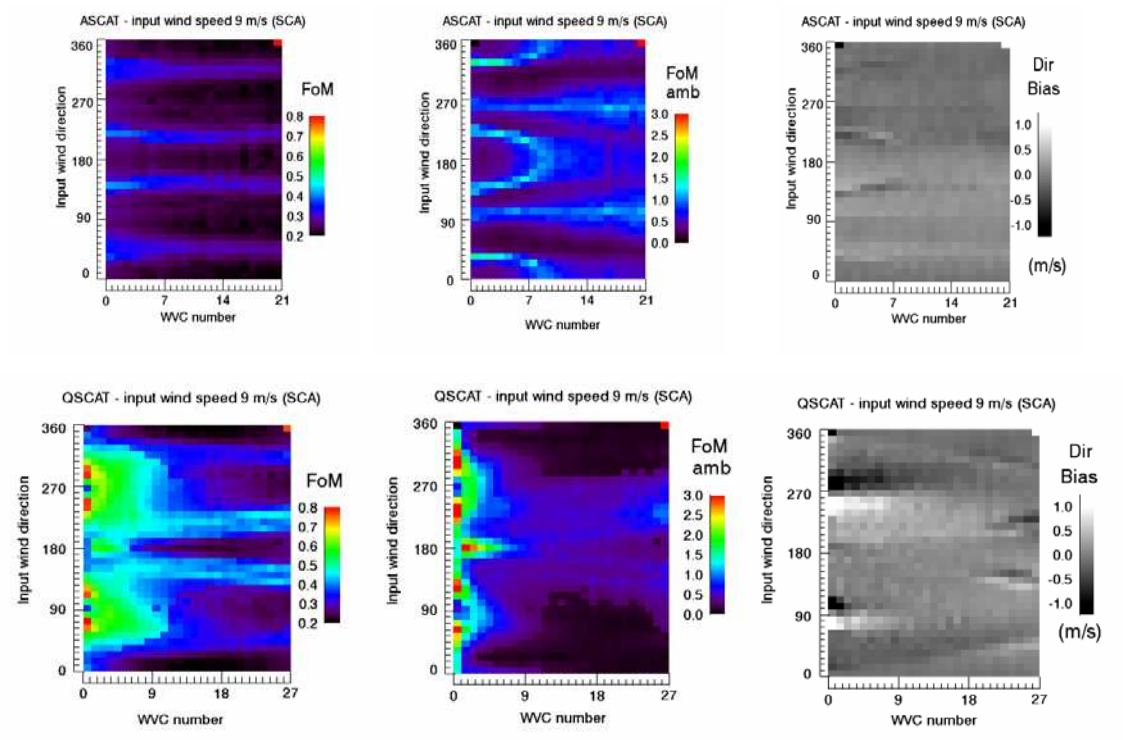

Figure 19 – QuikSCAT (top row) and ASCAT on *MetOp* (bottom row) SCA simulator FoMs as a function of across-track WVC location and wind direction (wind speed is 9 m/s)

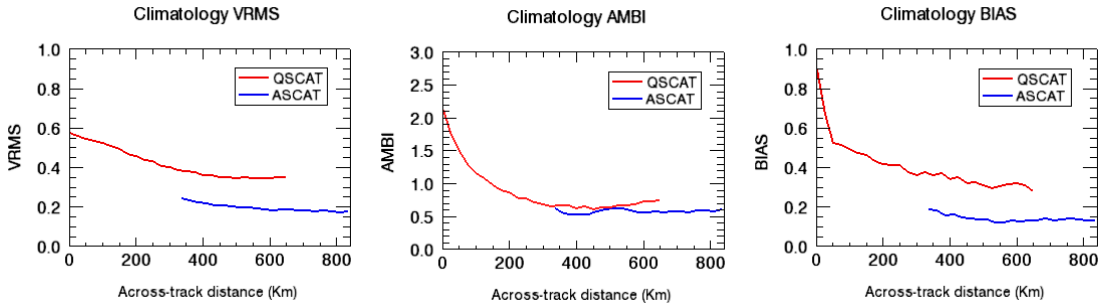

Figure 20 – Average climatology FoMs for QuikSCAT (red) and ASCAT on *MetOp* (blue) as a function of across-track distance

The average climatology FoM scores indicate that the quality of ASCAT winds is rather uniform across the scatterometer swath, with an average wind vector RMS error of 0.6 m/s. The wind vector RMS error is read from Eq. [9] as a function of the VRMS figure and the NWP background uncertainty (σ_{NWP}^2 = 5 m^2/s^2) as:

$$RMS_{obs} = FoM_{VRMS}\sqrt{2\sigma_{NWP}^2} \qquad [15]$$

In contrast, the QuikSCAT wind retrieval performance appears strongly dependent on across-track location with worst FoM scores at nadir locations and an average wind vector RMS error of 1.6 m/s. The QuikSCAT concept also seems to suffer from severe systematic errors in the retrieval of wind directions. Figure 21 illustrates the comparison between simulated wind direction biases (SCA simulator prediction with 9 m/s wind) and the observed long-term histograms (climatology) of quality-controlled QuikSCAT wind solutions archived at KNMI: systematic errors create directional preferences that finally make appearance as unnatural artifacts in the observed wind climatologies.

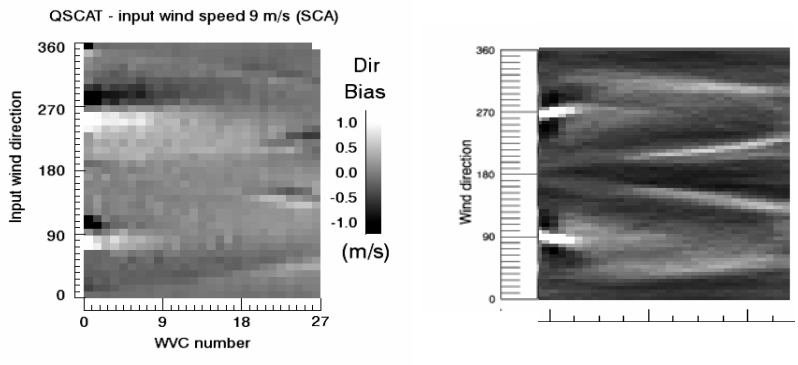

Figure 21 – Predicted bias (left) and observed histogram of output wind solutions (right) for QuikSCAT

4.2 Post-EPS scatterometer concepts (25 km)

Figures 22 to 24 summarize the performance figures for the Post-EPS ASCAT-type and RFSCAT-type scatterometer concepts elaborated by the Phase 0 industrial teams, labeled "Consortium 1" and "Consortium 2", using instrumental noise levels that comply with the mission requirements (i.e. Kp of 3 % at low incidence with allowance for linear degradation to 10 % for high incidence in the outer swath as in the Post-EPS MRD, see Appendix E) and geophysical noise levels adapted from ASCAT on *MetOp*. The Post-EPS ASCAT-type concept continues the series of C-band fixed fan-beam scatterometers and builds on *MetOp*'s ASCAT heritage, featuring an extended coverage towards smaller incidence angles (from 20 to 53.5 deg for the mid antennas) and an improved spatial resolution of 25 km. The RFSCAT-type concept can be regarded as a single ASCAT Mid-antenna spinning about the nadir axis at a rate such that largely overlapping footprints result between successive scans. Three different RFSCAT rotation rates have been considered in this study (1, 2 and 3 rpm).

Consortium 1

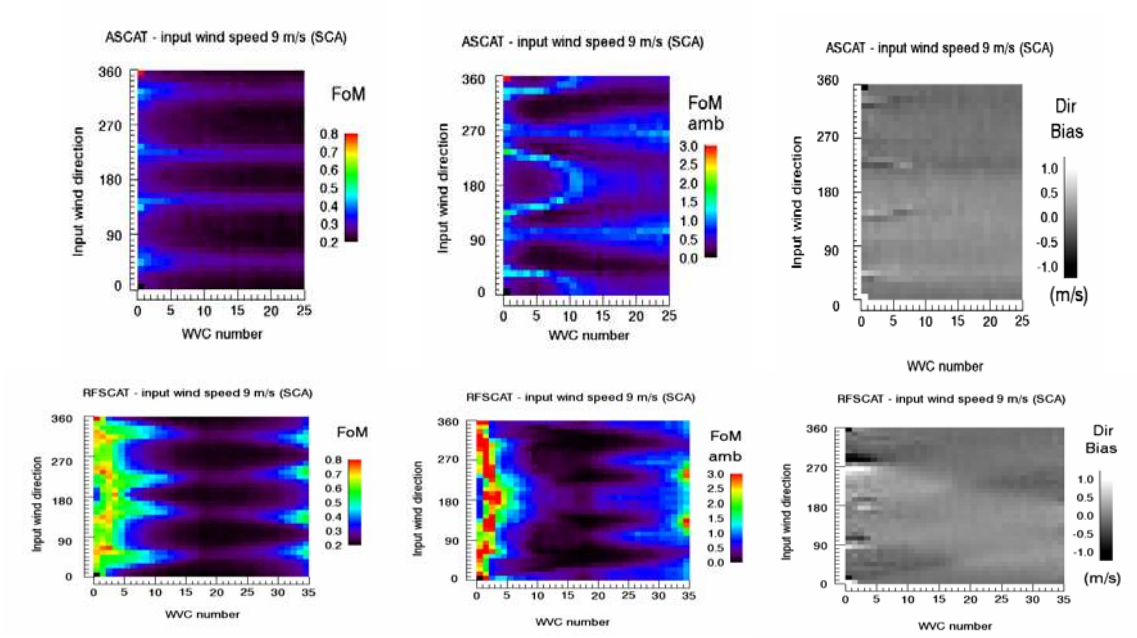

Figure 22 – Consortium 1: Post-EPS ASCAT-type (top row) and RFSCAT-type (2 rpm, bottom row) SCA simulator FoMs as a function of across-track location and wind direction (wind speed is 9 m/s)

FoM scores indicate that the wind quality of the Post-EPS ASCAT-type concept remains quite uniform across the swath (with similar performance to ASCAT on *MetOp*, with improved resolution), while that of the RFSCAT-type concept depends strongly on across-track location and degrades significantly at nadir and the swath edges. As with the rotating QuikSCAT, the RFSCAT-type concept suffers from poor observation geometry (reduced beam diversity in azimuth) at nadir and outer swath locations (with ensuing ambiguities and biases), although the geometry problem becomes alleviated when higher antenna rotation speeds are used. In any case, the extent of the comparably useful swath remains similar for both the fixed and rotating fan-beam concepts and is limited to about 650 km (single side) for a wind vector RMS error of 0.6 m/s. A definite strength of the RFSCAT-type concept lies in its very low ambiguity scores (low dependability on NWP background support for ambiguity removal) over the extent of its usable swath.

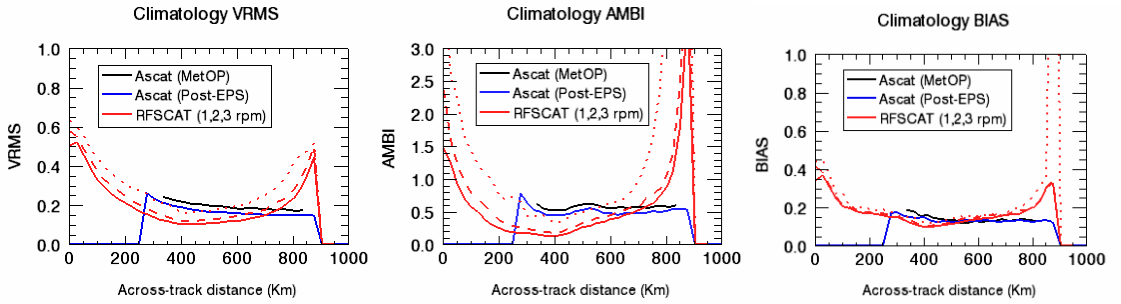

Figure 23 – Consortium 1: Average climatology FoMs for Post-EPS ASCAT-type concept (blue) and RFSCAT-type concept (red) as a function of across-track distance. ASCAT on *MetOp* is shown in black for reference.

Consortium 2

Only the ASCAT-type results are included for Consortium 2, as the complete RFSCAT-type model was not delivered in time.

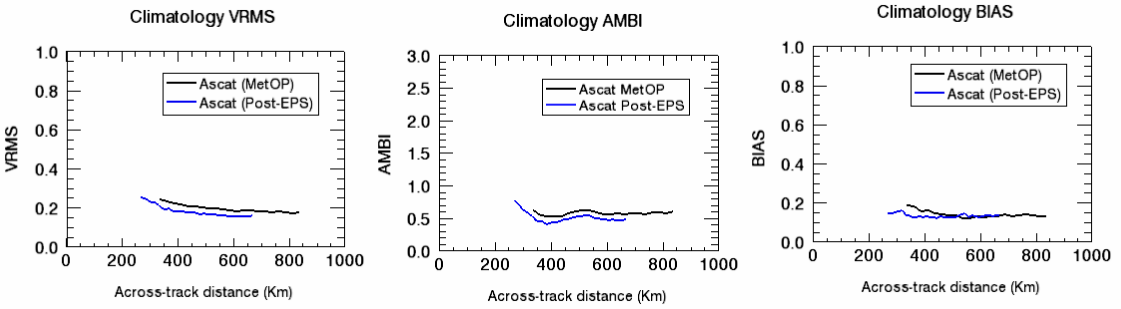

Figure 24 – Consortium 2: Average climatology FoMs for Post-EPS ASCAT-type concept (blue) as a function of across-track distance. ASCAT on *MetOp* is shown in black for reference.

Since the complementary strengths of active and passive observations for wind retrieval is a topic of interest, we would like to finish this study by plotting the performance figures of the Post-EPS ASCAT-type concept at low winds (< 8 m/s). These figures should allow direct comparison with the low wind retrieval performance of passive microwave techniques (e.g. WindSat).

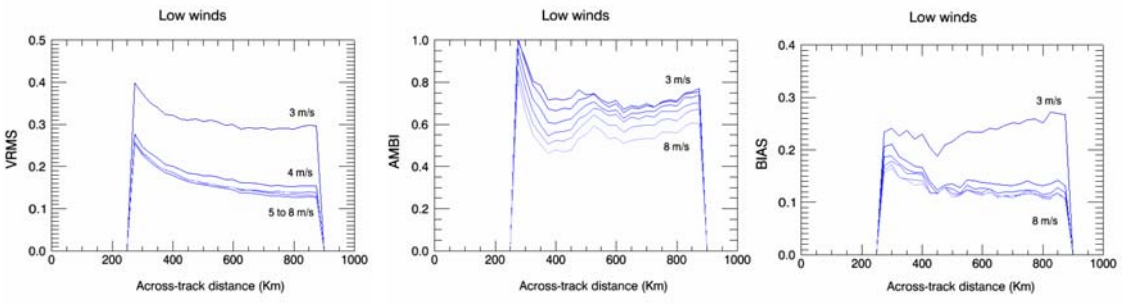

Figure 25 – Consortium 1: Low wind FoMs (< 8 m/s) for Post-EPS ASCAT-type concept as a function of across-track distance.

5 – Conclusion

A uniform and objective methodology for the performance assessment of dissimilar scatterometer concepts has been presented. The performance model rests on statistics produced by an end-to-end scatterometer wind retrieval simulator run in a Monte Carlo fashion. Several figures of merit have been proposed as a means to examine the different aspects that affect the quality of scatterometer wind products: the wind vector RMS error; the susceptibility to ambiguities; and the presence of biases. The performance model results, which reveal and quantify the inherent capabilities of different scatterometer configurations under realistic instrumental and geophysical noise conditions, have been validated using present day instruments such as SeaWinds on QuikSCAT and ASCAT on *MetOp*, and tested on future scatterometer concepts such as the rotating fan-beam (RFSCAT-type) concept. The performance model results indicate that the wind retrieval performance of the fixed beam ASCAT-type concept is rather uniform across the swath, while that of rotating concepts like SeaWinds or RFSCAT-type concepts remains strongly dependent on across-track location, degrading at nadir and the swath edges. Nevertheless, the performance of the RFSCAT-type concept is comparable to that of the ASCAT-type in terms of FoMs and usable swath extensions. The scatterometer performance model provides objective support to elaborate on different instrument configuration issues (including fixed or rotating antennas, number of azimuth views, radiometric performance, single or dual polarization

capabilities, and various pulse timing and ground-filter approaches) while monitoring the resulting wind quality. Lines of future work should include further progress in design sensitivity studies with respect to the usefulness of HH polarization at high wind speeds, the refinement of the scatterometer geophysical noise models, the assessment of wind retrieval performance in rainy scenarios, and the analysis of potential synergies between active and passive microwave observations, to name a few examples.

Appendices

Appendix A) Scatterometer observation geometries

To characterize a scatterometer backscatter vector completely, we need to define its observation angles as a function of location across the swath (see Figs. A.1, A.2 and A.3) and determine its measurement noise properties, namely the single look sensitivity (NESZ) and the number of looks and noise samples averaged per observation.

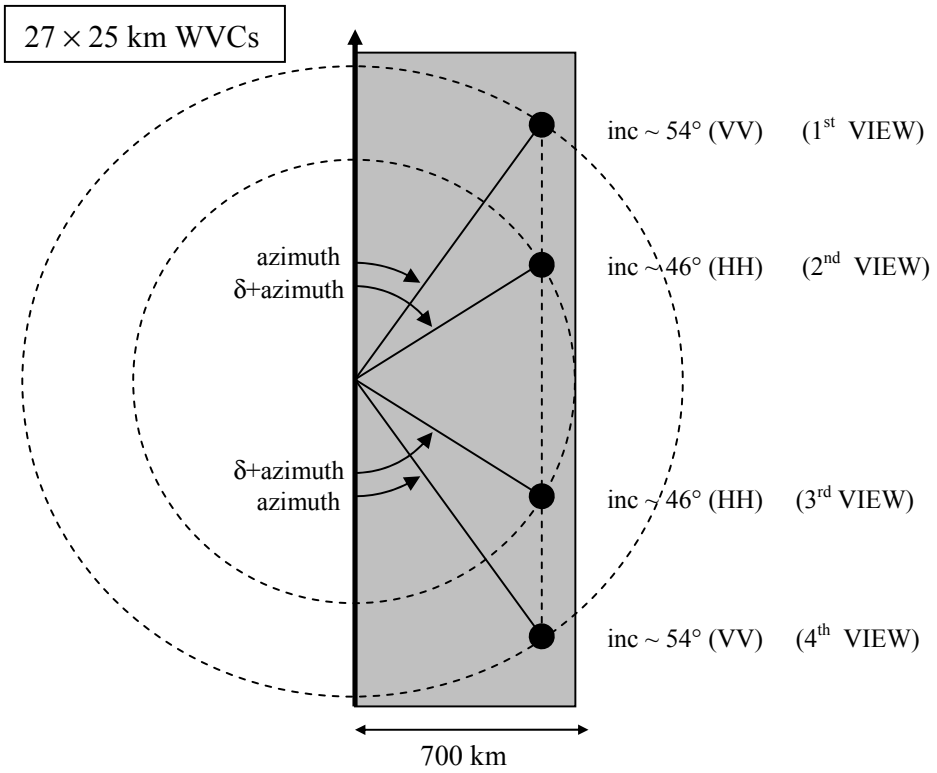

Figure A.1 – Observation geometry for QuikSCAT (satellite altitude = 800 km)

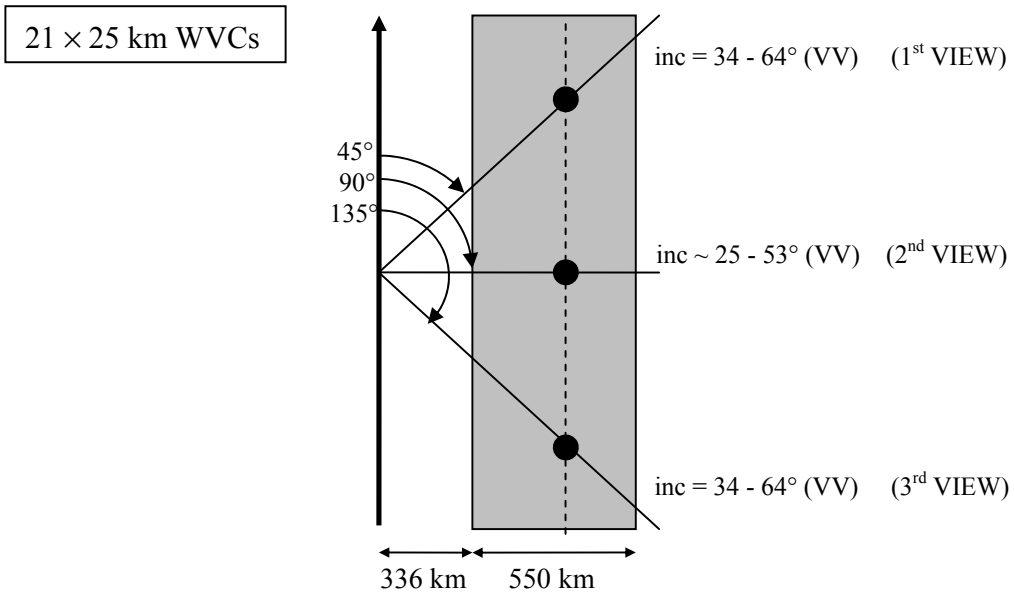

Figure A.2 – Observation geometry for ASCAT on *MetOp* (satellite altitude = 830 km)

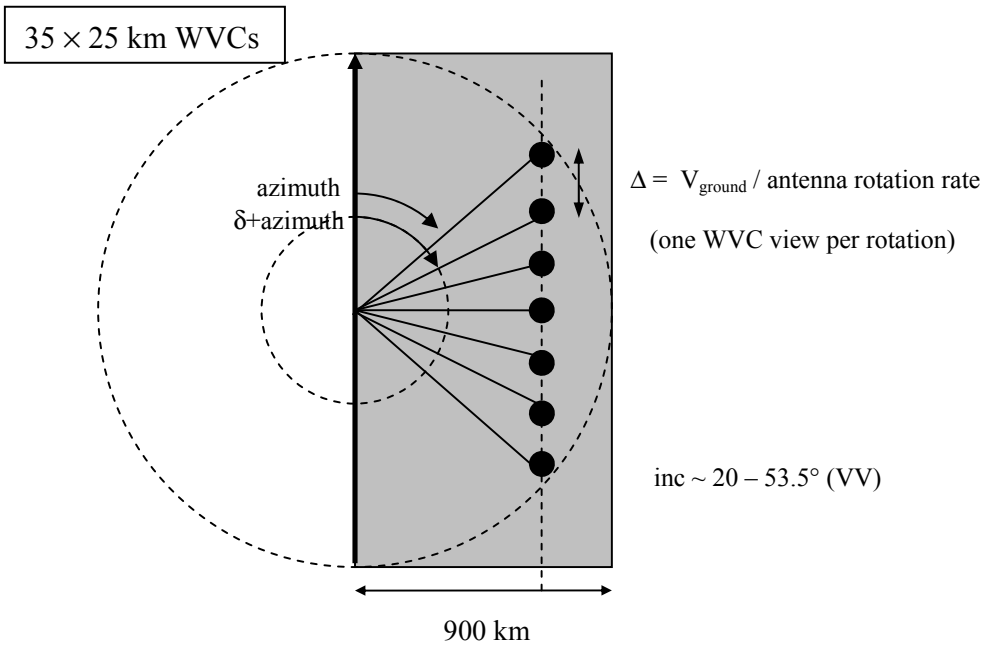

Figure A.3 – Observation geometry for RFSCAT (satellite altitude = 830 km)

Appendix B) Geophysical noise:

The scatterometer geophysical noise refers to perturbations in the backscatter vector components that arise from non-instrumental causes like sub-cell wind variability, atmospheric instability, confused sea-state, undetected rain or collocation errors within the WVC cell. Operationally, the geophysical noise is inferred from the observed variance of measurements across to the GMF, namely via the empirical normalization factors denoted <MLE>, used to force observed mean MLE values to be one prior to the quality control procedure [Portabella, 2006]. These <MLE> factors are calculated as a function of wind speed and WVC number and displayed in Fig.B.1 for the QuikSCAT and ASCAT instruments. Note that all <MLE> factors tend to one as wind speed increases, meaning that the measurement variance of strong surface returns is mainly driven by instrumental noise.

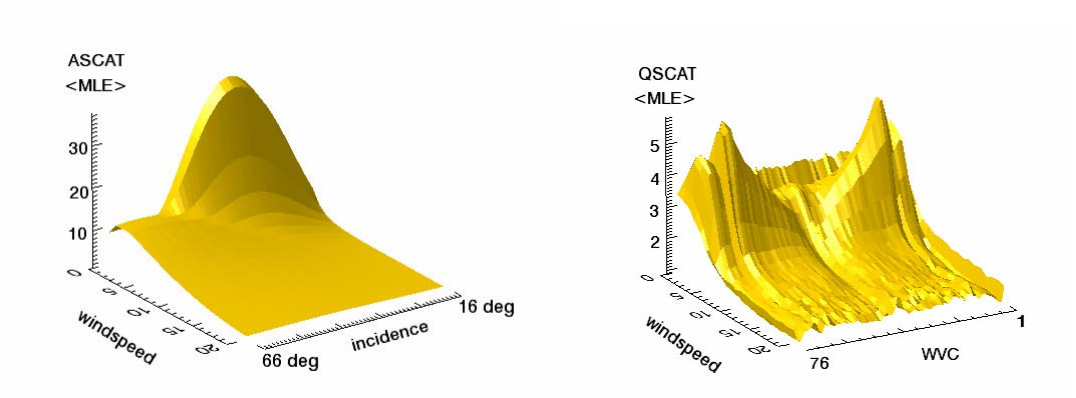

Figure B.1 –50 km resolution <MLE> tables for ASCAT (left) and QuikSCAT (right)

Recall that the normalized square distance MLE is constructed to guarantee that the variance of each residual component is unity:

$$MLE(\vec{v}\,|\,\sigma^0) = \frac{1}{\langle MLE \rangle} \sum_{i=1\ldots N} \frac{\left|\sigma_i^0 - \sigma_{GMF,i}^0(\vec{v})\right|^2}{k_{p,i}^2 \left(\sigma_i^0\right)^2} \qquad [B.1]$$

Where i is the beam index. The total variance of backscatter measurements across the GMF can be characterized by an effective k_{eff} such that

$$k_{eff,i}^2 = \langle MLE \rangle k_{p,i}^2 \qquad [B.2]$$

The geophysical noise model is constructed by assuming that the geophysical contribution to the backscatter variance is originated by an uncorrelated Gaussian process k_{geo} such that

$$k_{eff,i}^2 = k_{geo,i}^2 + k_{p,i}^2 \quad \Rightarrow \quad \langle MLE \rangle = 1 + k_{geo,i}^2 / k_{p,i}^2 \qquad [B.3]$$

Or equivalently

$$k_{geo}^2 = \left(\langle MLE \rangle - 1\right) \cdot k_p^2 \qquad \text{[B.4]}$$

The Ku-band geophysical noise model is estimated from the empirical QuikSCAT <MLE> tables (50 km resolution) as a function of wind speed and modeled as

$$k_{geo}(v) = 0.05 + 2.2 \cdot e^{-v/2} \qquad \text{[B.5]}$$

The C-band geophysical noise model is estimated from the empirical ASCAT <MLE> tables (50 km resolution) as a function of wind speed and modeled as

$$k_{geo}(v) = 0.12 \exp(-v/12) \qquad \text{[B.6]}$$

Scaling the C-band geophysical noise models down to 25 km resolution cells does not seem necessary, since the currently operational empirical ASCAT <MLE> table for 12.5 km gridded products at KNMI is very similar to the <MLE> table for 25 km grids. The ASCAT instrumental Kp noise levels at 12.5 and 25 km are also comparable. Therefore we use the same geophysical noise model for both the 50 km and 25 km resolution simulations at C-band.

To gain an appreciation for how geophysical noise affects the scatterometer performance figures, Figure B.1 shows the results from the SCA end-to-end simulator runs with and without geophysical noise. Observe that the geophysical noise contribution accounts for about a half of the simulated wind vector RMS error.

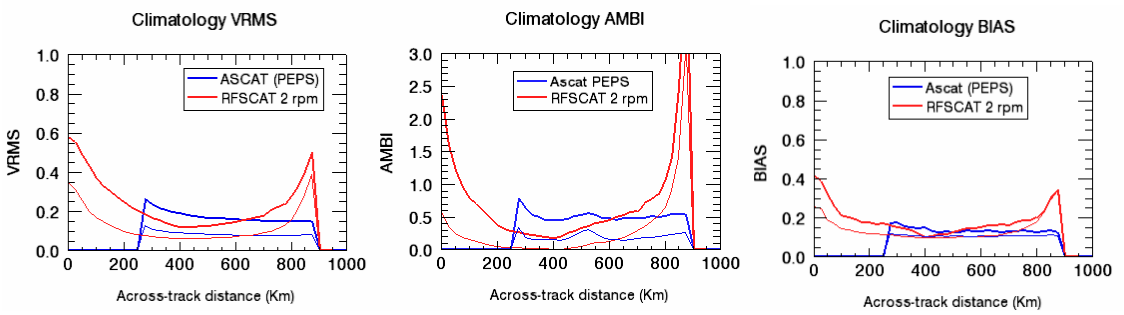

Figure B.1 – Consortium 1: Average climatology FoMs for Post-EPS ASCAT-type concept (blue) and RFSCAT-type concept (2 rpm, red) as a function of across-track distance with (thick line) and without (thin line) geophysical noise.

Appendix C) A note on Chi-Square distributions

A chi-square variable with k degrees of freedom is defined as the sum of the squares of k *independent* standard normal variables. If X_i are k independent, normally distributed random variables with mean 0 and variance 1, then the random variable

$$Q = \sum_{i=1,\ldots,k} X_i^2$$

is distributed according to the chi-square distribution with k degrees of freedom, which is usually written as $Q = \chi_k^2$. The probability density function of the chi-square distribution is

$$\chi_k^2(x) = \frac{1}{2^{k/2}\Gamma(k/2)} x^{k/2-1} e^{-x/2}$$

where Γ denotes the Gamma function.

Appendix D) A note on wind conventions

The antenna azimuth angles in Pseudo Level 1b files are measured clockwise from satellite heading. Unless specified otherwise, the wind angle convention in this report is Cartesian, namely counterclockwise from the axis of abscissas (across-track and looking right) and into the wind flow. The wind angle convention within the SCA simulator is meteorological (clockwise from north and opposite to flow, same as BUFR), although the input wind components are expressed in Cartesian components.

Appendix E) Post-EPS scatterometer design compliance with Kp requirements

This note evaluates the single look SNR levels and the compliance with Post-EPS radiometric Kp requirements of the scatterometer designs embedded in the Pseudo-L1b file input provided by the two Phase 0 industrial teams, labeled “Consortium 1” and “Consortium 2”. The min/max SNR and Kp levels correspond to 4 m/s cross-wind and 25 m/s up-wind conditions using the CMOD5 ocean backscatter model function (VV-pol). The single look SNR is computed as $SNR = \sigma^0/NESZ$. A recommended lower threshold value of SNR = -1.5 dB is used as reference. The Kp requirement threshold (i.e. Kp ≤ 0.175 × incidence – 1.375 for incidences larger than 25 degrees at 4 m/s cross-wind and Kp ≤ 3% at 25 m/s upwind) is used as a reference.

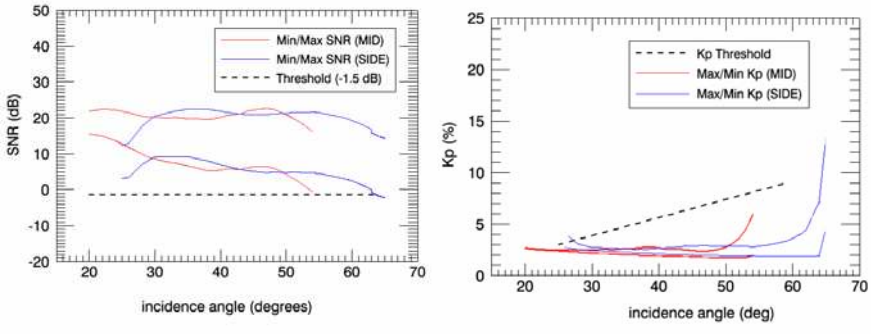

Figure E.1 – Consortium 1: ASCAT-type concept Kp compliance.

(Single look SNR left and radiometric Kp right)

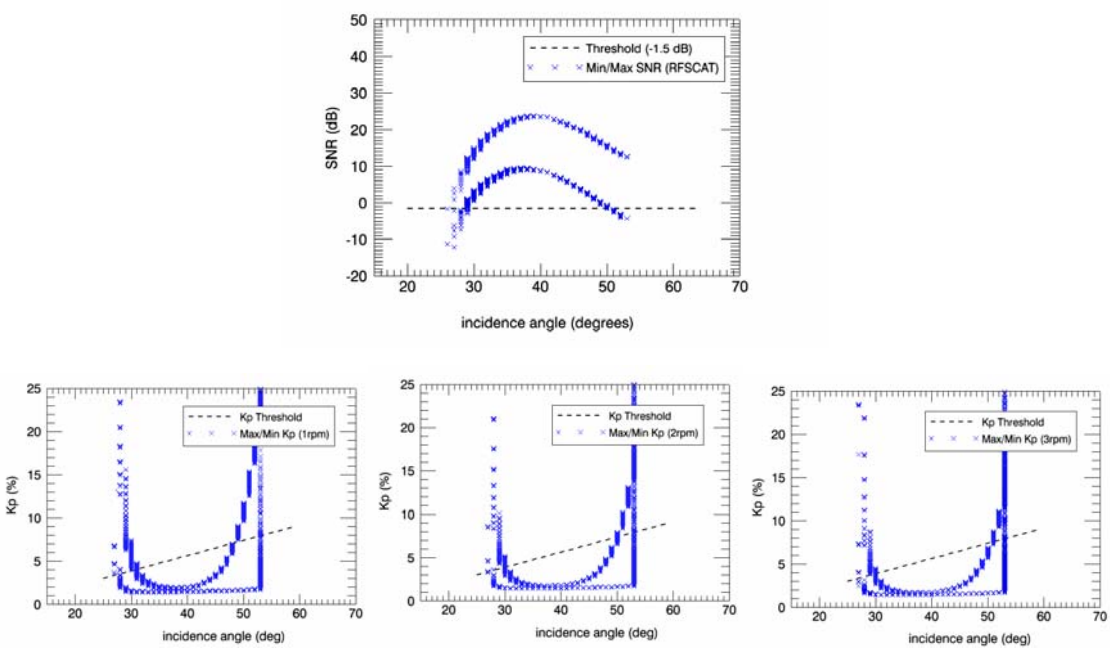

Figure E.2 – Consortium 1: RFSCAT-type concept Kp compliance.

(Single look SNR top and radiometric Kp bottom for 1, 2 and 3 rpm designs)

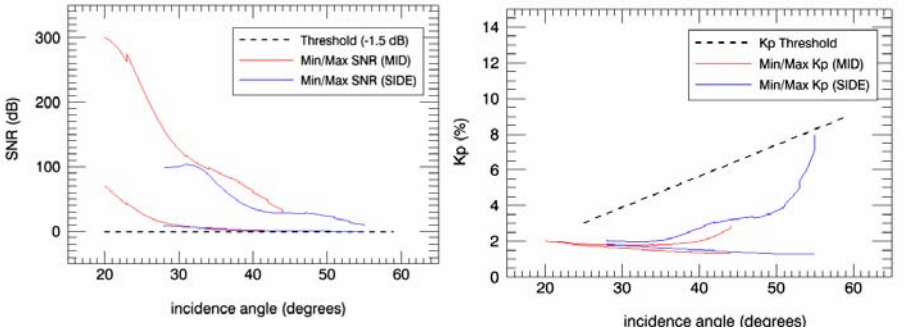

Figure E.3 – Consortium 2: ASCAT-type concept Kp compliance.

(Single look SNR left and radiometric Kp right)

References

[Fischer, 1972] Fischer, R.E., "Standard Deviation of Scatterometer Measurements from Space," IEEE Transaction on Geoscience Electronics, Vol. GE-10, No. 2, April 1972, pp. 106-113.

[Hersbach, 2007] Hersbach, H., A. Stoffelen and S. de Haan, "An Improved C-band scatterometer ocean geophysical model function: CMOD5", J. Geophys. Res., 112, 2007.

[Lin, 2002] Lin, C.C., A. Stoffelen, J. de Kloe, V. Wismann, S. Bartha, H.-R. Schulte, "Wind Retrieval Capability of Rotating, Range-Gated, Fanbeam Spaceborne Scatterometer", SPIE Int'l Symposium on Remote Sensing, 23-27 Sept. 2002, Crete, Greece.

[Liu, 2008] Liu, W. T., W. Tang, and X. Xie, "Wind power distribution over the ocean", *Geophys. Res. Lett.*, 35, L13808, doi:10.1029/2008GL034172, 2008.

[Portabella, 2006] Portabella, M., Stoffelen, A., "Scatterometer backscatter uncertainty due to wind variability", IEEE TGRS, 44(11), 2006.

[Stoffelen, 1998] A. Stoffelen, "Simulation of the wind performance of ASCAT", OSI-SAF Technical Note, 1998.

[Spencer, 2000] M.W. Spencer, C. Wu, D.G. Long, "Improved resolution backscatter measurements with the SeaWinds Pencil-Beam Scatterometer", IEEE TGRS, 38(1), 2000.

[Vogelzang, 2007] J. Vogelzang, "Two dimensional variational ambiguity removal (2DVAR)", Technical report NWPSAF-KN-TR-004, EUMETSAT, 2007.

[Vogelzang, 2009] J. Vogelzang, “Validation of two-dimensional variational ambiguity removal on SeaWinds Scatterometer data”, Journal of Atmospheric and Oceanic Technology, Vol/26, pp. 1229-1245, 2009.

[Wentz, 1999] F. J., Wentz, and D. K. Smith, “A Model Function for the Ocean-Normalized Radar Cross Section at 14 GHz Derived From NSCAT Observations”, J. Geophys. Res., 104(C5), 11499-11514, 1999.